CCI Land Surface Temperature

Climate Assessment Report
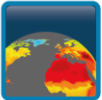
WP5.1 – DEL-CAR

Ref.: LST-CCI-D5.1-CAR
Date: 20-Dec-2021
Organisation: Consortium CCI LST
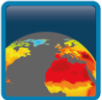
Signatures

	Name	Organisation	Signature
Written by	Lizzie Good, Freya Aldred	Met Office	
	Ruth Mottram, Jacob Høyer, Ioanna Karagali	DMI	
	Panagiotis Sismanidis, Benjamin Bechtel	RUB	
	Sophia Walther	MPI-BGC	
	Sorin Cheval, Alexandru Dumitrescu	MeteoRomania	
	Kaniska Mallick, Christian Bossung	LIST	
	Debbie Hemming, Rob King	Met Office	
	Raquel Niclòs	University of Valencia	
Reviewed by	Darren Ghent	ULeic	
Approved by	Darren Ghent	ULeic	
Authorized by	Simon Pinnock	ESA	

Change log

Version	Date	Changes
1.0	17-Dec-2020	First version
2.0	20-Dec-2021	Second version

Table of Content

List of Figures

List of Tables

Applicable Documents

Identity	Reference
AD-01	LST_cci (2020) Algorithm Development Plan, Reference LST-CCI-D2.4-ADP v2
AD-02	LST_cci (2020) Product Validation and Intercomparison Report, Reference LST-CCI-D4.1-PVIR v1

Reference Documents

Identity	Reference
RD-01	Squintu, A.A., van der Schrier, G., & van den Basselaar, E.J. (2019). EUSTACE / ECA&D: European land station daily air temperature measurements, homogenised. Retrieved 07 05, 2021, from European Climate Assessment & Dataset: https://catalogue.ceda.ac.uk/uuid/81784e3642bd465aa69c7fd40ffe1b1b
RD-02	Sen, P. K. (1968), Estimates of the regression coefficient based on Kendall's tau, J. Am. Stat. Assoc., 63, 1379–1389.
RD-03	Good, E. J., D. J. Ghent, C. E. Bulgin, and J. J. Remedios (2017), A spatiotemporal analysis of the relationship between near-surface air temperature and satellite land surface temperatures using 17 years of data from the ATSR series, J. Geophys. Res. Atmos., 122, 9185–9210, doi:10.1002/2017JD026880
RD-04	Vandecrux, B., Mottram, R., Langen, P. L., Fausto, R. S., Olesen, M., Stevens, C. M., Verjans, V., Leeson, A., Ligtenberg, S., Kuipers Munneke, P., Marchenko, S., van Pelt, W., Meyer, C. R., Simonsen, S. B., Heilig, A., Samimi, S., Marshall, S., Machguth, H., MacFerrin, M., Niwano, M., Miller, O., Voss, C. I., and Box, J. E.: The firn meltwater Retention Model Intercomparison Project (RetMIP): evaluation of nine firn models at four weather station sites on the Greenland ice sheet, The Cryosphere, 14, 3785–3810, https://doi.org/10.5194/tc-14-3785-2020, 2020.
RD-05	Fausto, R., van As, D., Box, J., Colgan, W. and Langen, P.: Quantifying the surface energy fluxes in South Greenland during the 2012 high melt episodes using in-situ observations, Frontiers in Earth Science, 4, 82, doi:10.3389/feart.2016.00082, 2016.
RD-06	Dybkjaer, G., Eastwood, S., Tonboe, R. T., Høyer, J., Borg, A. L., Englyst, P. N., … & Jensen, M. B. (2018). Arctic and Antarctic ice Surface Temperatures from AVHRR thermal Infrared satellite sensors, 1982-2015. AGUFM, 2018, GC24C-01.
RD-07	Høyer, J. L., & Karagali, I. (2016). Sea surface temperature climate data record for the North Sea and Baltic Sea. Journal of Climate, 29(7), 2529-2541.
RD-08	Nielsen-Englyst, P., Høyer, J. L., Madsen, K. S., Tonboe, R. T., & Dybkjær, G. (2019a). Deriving Arctic 2 m air temperatures over snow and ice from satellite surface temperature measurements. The Cryosphere Discussions, 1-31.
RD-09	Nielsen-Englyst, P., Høyer, J. L., Madsen, K. S., Tonboe, R., Dybkjær, G., & Alerskans, E. (2019b). In situ observed relationships between snow and ice surface skin temperatures and 2 m air temperatures in the Arctic. Cryosphere, 13(3), 1005-1024.
RD-10	Kurtz, N., Richter-Menge, J., Farrell, S., Studinger, M., Paden, J., Sonntag, J., & Yungel, J. (2013). IceBridge airborne survey data support Arctic sea ice predictions. Eos, Transactions American Geophysical Union, 94(4), 41-41.
RD-11	Langen, P. L., Mottram, R. H., Christensen, J. H., Boberg, F., Rodehacke, C. B., Stendel, M., van As, D., Ahlstrøm, A. P., Mortensen, J., Rysgaard, S., Petersen, D., Svendsen, K. H., Aðalgeirsdóttir, G. and Cappelen, J.: Quantifying energy and mass fluxes controlling Godthåbsfjord freshwater input in a 5 km simulation (1991-2012), Journal of Climate, 28(9), 3694–3713, doi:10.1175/JCLI-D-14-00271.1, 2015.
RD-12	Langen, P. L., Fausto, R. S., Vandecrux, B., Mottram, R. H. and Box, J. E.: Liquid Water Flow and Retention on the Greenland Ice Sheet in the Regional Climate Model HIRHAM5: Local and Large-Scale Impacts, Frontiers in Earth Science, 4, doi:10.3389/feart.2016.00110, 2017.
RD-13	Mottram, R., Boberg, F., Lang Langen, P., Yang, S., Rodehacke, C., Christensen, J. and Madsen, M.: Surface Mass balance of the Greenland ice Sheet in the Regional Climate

	Model HIRHAM5: Present State and Future Prospects, , 75, 105–115, doi:10.14943/lowtemsci.75.105, 2017.
RD-14	Høyer, J. L., Le Borgne, P., & Eastwood, S. (2014). A bias correction method for Arctic satellite sea surface temperature observations. Remote Sensing of Environment, 146, 201-213.
RD-15	Manoli, G., Fatichi, S., Bou-Zeid, E., & Katul, G. G. (2020). Seasonal hysteresis of surface urban heat islands. Proceedings of the National Academy of Sciences, 117(13), 7082–7089. https://doi.org/10.1073/pnas.1917554117
RD-16	Zhou, B., Rybski, D., & Kropp, J. P. (2013). On the statistics of urban heat island intensity. Geophysical Research Letters, 40(20), 5486–5491. https://doi.org/10.1002/2013GL057320
RD-17	Jung, M., C. Schwalm, M. Migliavacca, S. Walther, G. Camps-Valls, et al. (2020), Scaling carbon fluxes from eddy covariance sites to globe: synthesis and evaluation of the FLUXCOM approach, Biogeosciences, 17, 1343–1365, https://doi.org/10.5194/bg-17-1343-2020
RD-18	Papale, D., M. Reichstein, M. Aubinet, E. Canfora, C. Bernhofer, et al.(2006), Towards a standardized processing of Net Ecosystem Exchange measured with eddy covariance technique: algorithms and uncertainty estimation, Biogeosciences, 3, 571–583, https://doi.org/10.5194/bg-3-571-2006.
RD-19	Ermida, S. L., I. F. Trigo, C. C. DaCamara, A. C. Pires (2018), A Methodology to Simulate LST Directional Effects Based on Parametric Models and Landscape Properties, Remote Sensing, 10, 1114; doi:10.3390/rs10071114.
RD-20	Oke, T. (1973), City Size and the Urban Heat Island, Atmos. Environ., 7, 769-779, doi:10.1016/0004-6981(73)90140-6.
RD-21	Millard, S.P. (2013), EnvStats: An R Package for Environmental Statistics. Springer, New York. ISBN 978-1-4614-8455-4
RD-22	USEPA. (2006), Data Quality Assessment: A Reviewer's Guide. EPA QA/G-9R. EPA/240/B-06/002, February 2006. Office of Environmental Information, U.S. Environmental Protection Agency, Washington, D.C.
RD-23	Rosner, B. (1975), On the Detection of Many Outliers. Technometrics 17, 221–227.
RD-24	Mallick, K., Jarvis, A. J., Boegh, E., Fisher, J. B., Drewry, D. T., Tu, K. P., Hook, S. J., Hulley, G., Ardo, J., Beringer, J., Arain, A., and Niyogi, D.: A Surface Temperature Initiated Closure (STIC) for surface energy balance fluxes, Remote Sens. Environ., 141, 243–261, https://doi.org/10.1016/j.rse.2013.10.022, 2014.
RD-25	Mallick, K., Boegh, E., Trebs, I., Alfieri, J. G., Kustas, W. P., Prueger, J. H., Niyogi, D., Das, N., Drewry, D. T., Hoffmann, L., and Jarvis, A. J.: Reintroducing radiometric surface temperature into the Penman–Monteith formulation, Water Resour. Res., 51, 6214–6243, https://doi.org/10.1002/2014wr016106, 2015.
RD-26	Mallick, K., Trebs, I., Boegh, E., Giustarini, L., Schlerf, M., Drewry, D. T., Hoffmann, L., von Randow, C., Kruijt, B., Araùjo, A., Saleska, S., Ehleringer, J. R., Domingues, T. F., Ometto, J. P. H. B., Nobre, A. D., de Moraes, O. L. L., Hayek, M., Munger, J. W., and Wofsy, S. C.: Canopy-scale biophysical controls of transpiration and evaporation in the Amazon Basin, Hydrol. Earth Syst. Sci., 20, 4237–4264, https://doi.org/10.5194/hess-20-4237-2016, 2016.
RD-27	Mallick K, Toivonen E, Trebs I, Boegh E, Cleverly J, Eamus D, Koivusalo H, Drewry D, Arndt SK, Griebel A, Beringer J, and Garcia M (2018): Bridging Thermal Infrared Sensing and Physically-Based Evapotranspiration Modeling: From Theoretical Implementation to Validation Across an Aridity Gradient in Australian Ecosystems, Water Resources Research, 54, 3409–3435. https://doi.org/10.1029/2017WR021357 (open access).

RD-28	Gowik, U., and P. Westhoff (2011), The Path from C3 to C4 Photosynthesis, Plant Phys., 155(1), 56-63, doi:10.1104/pp.110.165308.
RD-29	Coll, C., Caselles, V., Galve, J.M., Valor, E., Niclòs, R., Sánchez, J.M., Rivas, R. (2005). Ground measurements for the validation of land surface temperatures derived from AATSR and MODIS data. Rem. Sens. Environ. 97, 288–300.
RD-30	Niclòs, R., Pérez-Planells, Ll., Valiente, J.A., Coll, C., Valor, E., 2018. Evaluation of the S-NPP VIIRS Land Surface Temperature product using ground data acquired by an autonomous system at a rice paddy. ISPRS J. Photogramm. Remote Sens. 135, 1-12.
RD-31	Wan, Z., Dozier, J., 1996. A generalized split-window algorithm for retrieving land-surface temperature from space. IEEE Trans. Geosci. Remote Sens. 34, 892–905.
RD-32	Wan, Z., 2014. New refinements and validation of the collection-6 MODIS land-surface temperature/emissivity product. Remote Sens. Environ. 140, 36–45.
RD-33	Gillespie, A.R., Matsunaga, T., Rokugawa, S., Hook, S.J., 1998. Temperature and emissivity separation from Advanced Spaceborne Thermal Emission and Reflection Radiometer (ASTER) images. IEEE Trans. Geosci. Rem. Sens. 36, 1113–1125.
RD-34	Hulley, G. C., S. J. Hook, and A. M. Baldridge (2011), Generating consistent land surface temperature and emissivity products between ASTER and MODIS data for Earth science research, IEEE Trans. Geosci. Remote Sens., 49(4), 1304–1315, doi:10.1109/TGRS.2010.2063034.
RD-35	Coll, C., Niclòs, R., Puchades, J., García-Santos, V., Galve, J.M., Pérez-Planells, Ll., Valor, E., Theocharous, E. (2019). Laboratory calibration and field measurement of land surface temperatura and emissivity using thermal infrared multiband radiometers. Int. J. Appl. Earth Obs. Geoinformation, 78, 227-239.
RD-36	Theocharous, E., N. P. Fox , I. Barker-Snook , R. Niclòs, V. Garcia Santos, P. J. Minnett, F. M. Göttsche, L. Poutier, N. Morgan , T. Nightingale, W. Wimmer, J. Høyer , K. Zhang , M. Yang , L. Guan, M. Arbelo, and C. J. Donlon (2019). The 2016 CEOS Infrared Radiometer Comparison: Part II: Laboratory Comparison of Radiation Thermometers. Journal of Atmospheric and Oceanic Technology, 1079–1092. 10.1175/JTECH-D-18-0032.1.
RD-37	Guillevic, P., Göttsche, F., Nickeson, J., Hulley, G., Ghent, D., Yu, Y., Trigo, I., Hook, S., Sobrino, J.A., Remedios, J., Román, M., Camacho, F. (2018). Land surface temperature product validation best practice protocol version 1.1. Best Pract. Satell. L. Prod. Valid. (p. 60) L. Prod. Valid. Subgr. doi, 58. https://doi.org/10.5067/doc/ceoswgcv/lpv/lst.001.
RD-38	Hulley, G.C., Hook, S.J., 2009. The North American ASTER Land Surface Emissivity Database (NAALSED). Version 2.0. Remote Sens. Environ., 113, 1967–1975.
RD-39	Good, E. (2016), An in situ-based analysis of the relationship between land surface 'skin' and screen-level air temperatures, J. Geophys. Res. Atmos., 121, 8801–8819, doi:10.1002/2016JD025318.
RD-40	Walther, S., Besnard, S., Nelson, J. A., El-Madany, T. S., Migliavacca, M., Weber, U., Ermida, S. L., Brümmer, C., Schrader, F., Prokushkin, A. S., Panov, A. V., and Jung, M.: Technical note: A view from space on global flux towers by MODIS and Landsat: The FluxnetEO dataset, Biogeosciences Discuss. [preprint], https://doi.org/10.5194/bg-2021-314, in review, 2021.https://bg.copernicus.org/preprints/bg-2021-314/

Executive Summary

This document represents the second Climate Assessment Report (CAR) for the LST_cci project (https://climate.esa.int/en/projects/land-surface-temperature/). It comprises reports from the six dedicated LST_cci project User Case Studies (UCS) and reports from other studies that have used beta versions of the LST_cci data sets produced during the first phase of the project. Some of these studies are still underway, but the feedback collected here is made available to the LST_cci Science Team to further develop and improve the LST_cci data sets and plan for the next phases of the project. Furthermore, most of the studies make use of v1.0 LST_cci products as the v2.0 LST_cci products were not available until near the end of the LST_cci phase I project. Early feedback presented in the CAR v1 has been instrumental in identifying some of the improvements implemented in v2.0 LST_cci products.

The overall user feedback on the beta LST_cci products is generally very positive:

❖ In general, users report the products are easy to use and are well described in netCDF format. Users comment that the common format for LST products from different sensors is very valuable, although benefit would be gained from further increasing consistency between products.

❖ Users appreciate the provision of additional fields in the files, such as viewing and solar geometry, and land cover class.

❖ Several of the studies reported here use Level 3 0.01° LST data; the provision of these higher-resolution data has been core to the success of these studies so far.

❖ A strong relationship between LSTs from LST_cci L3C v2.0 IR, SSMI_SSMIS_L3C v2.23 and MULTISENSOR_IRCDR_L3S v1.0 and collocated station 2m air temperature (T2m) observations is observed

❖ The Surface Urban Heat Island Intensity (SUHII) estimates and hysteretic cycles calculated from the 0.01° LST_cci custom products agree with those reported in the published literature using other products.

A number of issues that affect the utility of these data sets for climate applications have been identified by these early users. Many of these issues have already been addressed by the Science Team and are implemented in the v2.0 release. The main issues identified include:

❖ Non-climatic discontinuities in the multi-sensor infrared (IR) and microwave (MW) products

  ❍ Significant improvements have been made in the homogeneity of the LST_cci v2.0 products. However, discontinuities are still evident in some v2.0 products that require further improvement in future releases and in Phase II of the LST_cci project.

  ❍ Only the AQUA_MODIS_L3C and the ENVISAT_ATSR__L3C products appear stable; the TERRA_MODIS_L3C, ERS-2_ATSR__L3C, MULTISENSOR_IRCDR_L3S and SSMI_SSMIS_L3C products show non-climatic discontinuities associated with changes in sensor and/or drift over time.

❖ Issues relating to the averaging method used to create the L3 IR products where data are averaged over several orbits/timestamps that affects the utility of the data, particularly at high latitudes

  ❍ A recommendation is to provide both instantaneous and averaged LST fields (despite the fact that also the number of ancillary fields on observation time and angles and uncertainties will be multiplied).

A new approach has been implemented for the LST_cci v2.0 products where the observation closest to the nominal overpass time of the sensor has been used instead. This has improved comparisons to T2m observations and use in machine learning estimates of surface fluxes.

❖ Apparent cold biases in the MODIS retrievals over the Greenland ice sheet of at least several K but warm biases over a test site in Spain.

    ○ This is primarily due to the LST_cci v1.0 products using an older emissivity data set.

    ○ No emissivity values were provided in version 2 LST_cci MODIS L3C products (unlike in version 1 products) and emissivity is a key variable to obtain LST data so should be included.

The LST_cci v2.0 products uses an improved data set, which is expected to resolve many of these 'bias' issues. For Greenland in particular the implementation of an enhanced cloud masking scheme is expected to significantly reduce the cold biases. The LST_cci Science Team will look to including emissivity as an output variable in future releases.

❖ Residual cloud contamination in the IR data sets (severe for some data sets)

    ○ Some of this cloud contamination is due to a bug in the processor, which has now been resolved. Cloud masking has been improved in the LST_cci v2.0 products through the use of a probabilistic cloud detection scheme.

    ○ However, residual cloud contamination still remains and advice on how to deal with this when using the data would be appreciated.
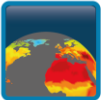
The LST_cci Science Team will be looking at post processing filtering for residual cloud contamination, as well as further effort towards cloud algorithm improvements, in Phase-2.

❖ Difficulty in using the LST_cci 0.01° data due to the way the data are delivered to users

    ○ The Greenland UCS appreciated a special data delivery of Level 2 swath observations which worked well to allow analysis in this high latitude region where it is not feasible to divide products into ascending and descending.

    ○ For Urban Heat Island studies, the main difficulty encountered in processing the LST_cci data was the mosaicking and stacking of the daily data over large regions; it would be very useful if the data from each orbit were mosaicked beforehand and provided as tiles.

    ○ Naming the LST_cci tiles with a geo-location would be helpful or providing with a clear identification according to the MODIS tiling system or for example the Sentinel-2 tile grid (UTM system). This would make the identification of tiles containing the LST_cci data of the areas of interest easier.

    ○ The different presentation of IR and MW data into day/night and ascending/descending also makes analysis more challenging in some applications.

Improved delivery of LST_cci data is currently being developed by the Science Team; a command line tool for re-gridding and sub-setting to user defined resolutions will be available at end of 1st Quarter 2022.

❖ Use of the SEVIRI product would be aided by provision of the full record and inclusion of a geometrical correction factor for nadir view in the files (although it is acknowledged that the desirable reference angle might differ between applications).

In addition, several minor issues/errors within the LST_cci data files have also been identified, for example, errors in some of the attribute names (e.g. repetition of latitude, rather than latitude and

longitude), presenting static land cover rather than dynamic information and differences between the quality and auxiliary information presented in the IR and MW data files. Regular communication between the Climate Research Group (CRG, which comprise the UCS and other users) and the Science Team has ensured that these issues have been resolved quickly.

A list of further recommendations or areas for development to be considered in future years of the LST_cci project is also presented in this report.

The User Case Studies have provided highly relevant feedback for the Science Team to improve the performance of the LST_cci products. The Science Team have in parallel been working on improvements to these products for the first data release to the CCI Open Data Portal and have taken on board feedback from the CRG throughout the progress of the User Case Studies. While the focus of this report is on an independent climate assessment of the LST_cci products details information on the wider context of how the project is responding to the feedback is also provided.

1. Introduction

1.1 Purpose and scope

The European Space Agency's (ESA's) Climate Change Initiative (CCI) project aims to provide a comprehensive and timely response to the challenging requirements set by the Global Climate Observing System (GCOS) and the Committee on Earth Observation Satellites (CEOS) for highly stable, long-term, satellite-based products for climate research.

Space observations provide unique information that cannot be obtained from traditional ground stations – they can provide better spatial coverage and resolution, and records are now approaching the time periods required for climate research. As part of the CCI project, a total of 22 Essential Climate Variables (ECVs) have been targeted. Fourteen of these ECVs were included in the first phase of ESA's CCI project. A further eight have been selected for the second phase of the project, which includes Land Surface Temperature (LST). The LST_cci project aims to deliver a significant improvement on the capability of current satellite LST data records to meet the GCOS requirements for climate applications and realise the full potential of long-term LST data for climate science (https://climate.esa.int/en/projects/land-surface-temperature/).

Now in its final year of Phase-1, the LST_cci project has produced beta products for a range of satellites that include instruments operating at both infrared (IR) and microwave (MW) wavelengths, and in polar-orbiting and geostationary orbit (Table 1-1). Version 1 (v1) of these beta products were delivered just after the end of the first year of the project. They were made available to selected users who are performing dedicated user case studies (UCS) that are funded through the LST_cci project, users from other CCI projects (e.g. permafrost_cci) and the CCI Climate Modelling User Group (CMUG), and other interested parties who are in direct contact with the LST_cci science team. Such trailblazer users are critical to the success of the project as they can provide early feedback and assessment of the LST_cci data sets that can be used to improve the products while they are being developed and before they are officially released to the wider public. Version 2 (v2) products for many sensors were made available in year 3 of the project. Many of the improvements made to the v2 products compared with v1 were a result of the feedback from the trailblazer users.

As ESA's CCI project targets the production of data sets that can be used for climate research, a crucial requirement is to assess the suitability and utility of these data from a climate-science perspective. Across CCI, this is performed through the Climate Assessment Reports (CAR) that are produced by each CCI project. This document presents the CAR version 2.0 (v2.0) for the LST_cci project. The objective of the report is to provide information on the suitability of the beta LST_cci data products for climate applications. This CAR focuses on both climate-critical aspects of the data, such as stability and homogeneity, and the utility and presentation of the data in a way that is useful for climate applications. The assessment is based on reports from the User Case Studies (UCS) funded through the LST_cci project and other studies that are not directly funded through the project. **However, it should be noted that some of the studies reported here, including four of the six UCS, utilise customised 0.01° v1 LST_cci data and therefore the significant updates that have been made in the v2 LST_cci datasets are not yet reflected in these studies.** The data version used in each study is indicated clearly in each case.

1.2 Structure of the document

This document consists of three sections. Section 2 presents the reports from the six UCS that are part of the LST_cci project, while Section 3 presents reports from other studies that have used the LST_cci beta products. For both sets of reports, the scientific objectives of the study are outlined together with a brief description of the study approach and results. Feedback on the utility of the LST_cci data from each study is also provided. Section 4 of the report synthesises the findings from all studies presented in Section 2 and Section 3 and summarises the main outcomes of this CAR.

1.3 Definition of terms

The terms used in this report are listed below, together with their definitions.

Term	Definition
AASTI	Arctic and Antarctic ice Surface Temperatures from thermal Infrared satellite sensors
AATSR	Advanced Along-Track Scanning Radiometer
ATSR	Along-Track Scanning Radiometer
ATSR-2	Second ATSR instrument
AVHRR	Advanced Very High Resolution Radiometer
C3	C3 Plant Functional Type
C4	C4 Plant Functional Type
CAR	Climate Assessment Report
CCI	Climate Change Initiative
CDR	Climate Data Record
CEOS	Committee on Earth Observation Satellites
CMIP6	Climate Model Intercomparison Project 6
CMUG	Climate Modelling User Group
CRG	Climate Research Group
DMI	Danmarks Meteorologiske Institut (Danish Meteorological Institute)
DMSP	Defense Meteorological Satellite Program
E	Evapotranspiration
E_E	Evaporation
E_T	Transpiration
EC	Eddy Covariance
ECV	Essential Climate Variable
EOS	Earth Observing System

ERA5	ECMWF Reanalysis 5
ERS-2	Second European Remote Sensing satellite
ESA	European Space Agency
ESM	Earth System Model
EUSTACE	EU Surface Temperature for All Corners of Earth
FCDR	Fundamental Climate Data Record
GCOS	Global Climate Observing System
H	Sensible heat flux
IPCC	Intergovernmental Panel on Climate Change
IR	InfraRed
IST	Ice Surface Temperature
K	Kelvin
L3	Level 3
L4	Level 4
L3C	Level 3C
LC	Land Cover
LC_cci	Land Cover Climate Change Initiative
LCC	Land Cover Class
LE	Latent heat flux
LST	Land Surface Temperature
LIST	Luxemburg Institute of Science and Technology
LSA SAF	Satellite Application Facility on Land Surface Analysis
LST_cci	Land Surface Temperature Climate Change Initiative
m	Slope / gradient of a straight line
MeteoRomania	National Meteorological Administration of Romania
MODIS	Moderate Resolution Imaging Spectroradiometer
MOHC	Met Office Hadley Centre
MPI-BGC	Max Planck Institute for Biogeochemistry
MPW	Median of Pairwise Slopes
MSG	Meteosat Second Generation
MSLP	Mean Sea-Level Pressure
MW	MicroWave
NASA	National Aeronautics and Space Administration (USA)

NATT	North Australian Tropical Transect
netCDF	Network Common Data Format
NOAA	National Oceanic and Atmospheric Administration (USA)
PUG	Product User Guide
r	Pearson correlation coefficient
RCM	Regional Climate Model
RetMIP	Retention Model Intercomparison Project
RMS	Root Mean Square
RUB	Ruhr-University Bochum
S_T	Water stress
SATAZ	Satellite Azimuth Angle
SATZE	Satellite Zenith Angle
SEB	Surface Energy Balance
SEVIRI	Spinning Enhanced Visible and Infra-Red Imager
SLSTR	Sea and Land Surface Temperature Radiometer
SM_cci	Soil Moisture Climate Change Initiative
SMB	Surface Mass Balance
SSM/I	Special Sensor Microwave/Imager
SSMIS	Special Sensor Microwave Imager Sounder
STIC	Surface Temperature Initiated Closure
SUHI	Surface Urban Heat Island
SUHII	Surface Urban Heat Island Intensity
T2m	2m air temperature
UCS	User Case Study
UKESM	UK Earth System Model
UHI	Urban Heat Island
WMO	World Meteorological Organisation

Table 1-1: LST_cci products available to the CRG / CMUG in compilation of the CAR.

Product String	Version	Instrument	LST_cci ID	Satellite	Spatial Resolution	Temporal Resolution	Data Availability	Data Accessibility (Workspace)
ERS-2_ATSR__L2P	1.00, 2.00	ATSR-2	ATSR_2	ERS-2	1 km swath	Full orbit	1995 – 2003	Private (leicester)
ERS-2_ATSR__L3C					0.05° global lon-lat grid	Daily / Month – Day + Night		Public (esacci_lst)
ENVISAT_ATSR__L2P	1.00, 2.00	AATSR	ATSR_3	Envisat	1 km swath	Full orbit	2002 – 2012	Private (leicester)
ENVISAT_ATSR__L3C					0.05° global lon-lat grid	Daily / Month – Day + Night		Public (esacci_lst)
TERRA_MODIS_L2P	1.00, 2.00	MODIS	MODIST	EOS Terra	1 km swath	5 minute granules	2000 – 2018	Restricted (nceo_generic)
TERRA_MODIS_L3C					0.05° global lon-lat grid	Daily / Month – Day + Night		Public (esacci_lst)
AQUA_MODIS_L2P	1.00, 2.00	MODIS	MODISA	EOS Aqua	1 km swath	5 minute granules	2002 – 2018	Restricted (nceo_generic)
AQUA_MODIS_L3C					0.05° global lon-lat grid	Daily / Month – Day + Night		Public (esacci_lst)
SENTINEL3A_SLSTR_L2P	1.00, 2.00	SLSTR	SLSTRA	Sentinel 3A	1 km swath	3 minute granules	2016 – 2018	Private (leicester)
SENTINEL3A_SLSTR_L3C					0.05° global lon-lat grid	Daily / Month – Day + Night		Public (esacci_lst)
SENTINEL3B_SLSTR_L2P	1.00, 2.00	SLSTR	SLSTRB	Sentinel 3B	1 km swath	3 minute granules	2018 – 2020	Private (leicester)
SENTINEL3B_SLSTR_L3C					0.05° global lon-lat grid	Daily / Month – Day + Night		Public (esacci_lst)
MSG_SEVIRI_L3U	1.01	SEVIRI	SEVCCI	Meteosat	0.05° regional lon-lat grid	Hourly	2008 – 2010	Public (esacci_lst)
SSMI_SSMIS_L3C	V2.23	SSM/I + SSMIS	SSMI13 / SSMI17 / SSMI18	DMSP	0.25° global lon-lat grid	Daily – Ascending + Descending	1995 - 2018	Public (esacci_lst)
MULTISENSOR_IRCDR_L3S	1.00	ATSR-2 + AATSR	ATSR_2 / ATSR_3	ERS-2 + Envisat	0.05° global lon-lat grid	Daily / Month – Day + Night	1995 - 2012	Public (esacci_lst)

All Level-3C data can be accessed on the JASMIN "Public" partition of the "esacci_lst" workspace through the link: http://gws-access.jasmin.ac.uk/public/esacci_lst/

Data on the "Private" and "Restricted" (requires authorisation) workspaces are stored on these based entirely on data storage requirements for Level-2 data.

Note, the data products listed in Table 1-1 represent those used by the CRG / CMUG in the compilation of the CAR and are not reflective of the final LST_cci data products being released onto the CCI Open Data Portal at the end of Phase-1.

2. LST_cci User Case Study Reports

2.1 Regional and Global Trends in LST: A Stability Assessment of the LST_cci Products (Met Office)

2.1.1 Key Messages

❖ A strong relationship between LSTs from LST_cci L3C v2.0 IR, SSMI_SSMIS_L3C v2.23 and MULTISENSOR_IRCDR_L3S v1.0 and collocated station 2m air temperature (T2m) observations is observed (LST vs T2m anomaly correlations and slopes range between 0.6 and 0.9).

❖ This relationship is used to assess the temporal stability of all L3C and the MULTISENSOR_IRCDR_L3S LST_cci products to determine if they are sufficiently stable for climate trend detection.

❖ Only the AQUA_MODIS_L3C and the ENVISAT_ATSR__L3C products appear stable; the TERRA_MODIS_L3C, ERS-2_ATSR__L3C, MULTISENSOR_IRCDR_L3S and SSMI_SSMIS_L3C products show non-climatic discontinuities associated with changes in sensor and/or drift over time.

❖ For AQUA_MODIS_L3C (2002-2018), significant trends in LST of 0.64-0.66 K/decade are obtained, which compare well with the equivalent T2m trends of 0.52-0.59 K/decade. The LST and T2m trends for ENVISAT_ATSR__L3C (2002-2012) are found to be statistically insignificant, likely due to the comparatively short analysis period and specific years available for analysis.

❖ The LST_cci products are generally very useful and easy to use, although there are some minor issues with the data format (mistakes) and some possible cloud contamination in the MODIS data.

2.1.2 Scientific Analysis

2.1.2.1 Aims of the study

Trends in 2m air temperature (T2m) are well established and are a key metric for understanding climate change. T2m observations are obtained from a network of weather stations across the globe, which can be sparse in some regions such as Africa and Greenland. This leads to gaps in the derived datasets and therefore larger uncertainties in the estimated trends. If sufficiently stable in time, satellite-observed Land Surface Temperatures (LST) provide useful complementary observations now that multidecadal records are available. LST can provide independent information on changes in surface temperature where T2m observations exist and new information where T2m observations are unavailable.

The objective of this study is to assess the stability and trends in the LST_cci datasets, and to compare them with equivalent trends in T2m. The LST data are first compared with homogenized station T2m data to verify that the relationship between LST and T2m that has been found in other studies is also evident using the LST_cci data sets. The temporal stability of the LST_cci data is then assessed by comparing the time series of LST with the homogenized T2m data, where any differences are assumed to indicate non-climatic discontinuities in the LST_cci datasets. Finally trends in both the LST and T2m data are calculated and compared. In addition, the open question concerning how trends in IR LST are affected by using only cloud-free observations, the so-called 'clear-sky bias' effect, is also examined in this study.

2.1.2.2 Data and Methods

The LST datasets used for this study are summarised in Table 2-1. All the InfraRed (IR) datasets are daily with separate fields for daytime (LST$_{day}$) and night-time (LST$_{night}$) overpasses for the IR products. The overpass time is different for each instrument, but this is stable for each IR instrument during its lifetime. For the multi-sensor product, which comprises ATSR-2 and AATSR, the overpass time for the ATSR-2 data (10:30 am/pm) has been corrected to the overpass time of the AATSR (10:00 am/pm). The SSMI_SSMIS_L3C MicroWave (MW) product is also daily, but with separate fields for ascending (LST$_{asc}$) and descending (LST$_{desc}$) overpasses, rather than daytime and night-time due to the overpass time and orbital drift. The correction available in the product to adjust the overpass time to a nominal 6:00am/pm is applied in this study.

Table 2-1: A summary of LST_cci products used for this case study.

Product String and version	Sensor type	Resolution	Data availability	Local time of ascending node
ERS-2_ATSR__L3C v2.0	IR	0.05°	August 1995 – June 2003	22:30
ENVISAT_ATSR__L3C v2.0	IR	0.05°	July 2002 – April 2012	22:00
TERRA_MODIS_L3C v2.0	IR	0.05°	February 2000 – December 2018	22:30
AQUA_MODIS_L3C v2.0	IR	0.05°	July 2002 – December 2018	13:30
MULTISENSOR_IRCDR_L3S v1.0	IR	0.05°	August 1995 – March 2012	22:00 (ATSR-2 overpass time adjusted to AATSR)
SSMI_SSMIS_L3C v2.23	MW	0.25°	January 1995 – December 2020	~17:30-19:30 but corrected to 18:00
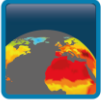
The relationship between LST and T2m, and the stability of the LST_cci data sets is assessed using homogenised daily minimum (T$_{min}$), maximum (T$_{max}$) and mean (T$_{mean}$) T2m data provided by the EU Surface Temperature for All Corners of Earth (EUSTACE: https://www.eustaceproject.org/) for meteorological stations within Europe and the Mediterranean [RD-01]. The gridded LST_cci products are spatially and temporally collocated with EUSTACE station locations. For the IR products, LST$_{night}$ and LST$_{day}$ are compared to T$_{min}$ and T$_{max}$ respectively. For the SSMI_SSMIS_L3C product, the LST$_{desc}$ (~6 am) is compared to T$_{min}$ and LST$_{asc}$ (~6 pm) is compared to T2m$_{max}$; daily mean LST (LST$_{mean}$), calculated from the mean of LST$_{night}$ and LST$_{day}$ or LST$_{desc}$ and LST$_{asc}$, is also compared to T$_{mean}$.

Climatologies are calculated for the LST and T2m time series separately, for each station location, based on a 31-day moving median window calculated for each calendar day of the year. This is done for each of the satellite time periods so equivalent LST/T2m datasets can be compared. The median station climatology is then subtracted from the observed data to calculate the following anomaly time series:

Equation 2-1 $\quad LST_{day\_anom} = LST_{day\_observed} - LST_{day\_climatology}$

Equation 2-2 $\quad LST_{night\_anom} = LST_{day\_observed} - LST_{day\_climatology}$

Equation 2-3 $\quad LST_{desc\_anom} = LST_{desc\_observed} - LST_{desc\_climatology}$

Equation 2-4 $LST_{asc\_anom} = LST_{asc\_observed} - LST_{asc\_climatology}$

Equation 2-5 $LST_{mean\_anom} = LST_{mean\_observed} - LST_{mean\_climatology}$

Equation 2-6 $T_{max\_anom} = T_{max\_observed} - T_{max\_climatology}$

Equation 2-7 $T_{min\_anom} = T_{min\_observed} - T_{min\_climatology}$

Equation 2-8 $T_{mean\_anom} = T_{mean\_observed} - T_{mean\_climatology}$

The relationship between LST and T2m anomalies (LST anomaly vs T2m anomaly) is assessed at each station by calculating the Pearson correlation coefficient (*r*), and the slope (*m*) using the Median of PairWise (MPW) slopes [RD-02]. A value of unity for both these parameters indicates a perfect relationship at that location.

To assess the stability of the products, monthly mean anomalies are calculated for LST and T2m using only temporally matched observations that are available in both datasets. A time series of differences is then calculated as:

Equation 2-9 $Difference_{day\_anom} = LST_{day\_anom} - T_{max\_anom}$

Equation 2-10 $Difference_{night\_anom} = LST_{night\_anom} - T_{min\_anom}$

Equation 2-11 $Difference_{desc\_anom} = LST_{desc\_anom} - T_{min\_anom}$

Equation 2-12 $Difference_{asc\_anom} = LST_{asc\_anom} - T_{max\_anom}$

Equation 2-13 $Difference_{mean\_anom} = LST_{mean\_anom} - T_{mean\_anom}$

Where the confidence interval of the slope of time series of anomaly differences does not encompass zero, the slope is considered to be statistically significant. Trends in both LST and T2m anomaly time series are also calculated using the MWP slopes, which is more robust to outliers than conventional linear regression [RD-02].

2.1.2.3 Results

An initial comparison with T2m is performed using homogenized T2m at a number of station locations across Europe. Co-locating satellite observed LST data with the stations results in between 221 and 651 comparison locations for the six different LST_cci datasets. LST and T2m anomalies (LST vs T2m) are found to compare well with consistent slopes (*m*) and correlations (*r*). For comparisons with T_{max} and T_{mean} values of ~0.8 and ~0.9 K/K are obtained for *r* and *m*, respectively, while T_{min} comparison values are closer to ~0.6 for both parameters. These are similar to the results of Good et al. (2017) [RD-03], who compared anomalies from an ATSR-2/AATSR climate data record with gridded T2m observations.   The T_{min} comparisons generally exhibit a higher variance than the T_{max} and T_{mean} comparisons (Table 2-2). Slopes of <1 indicate that anomalies in LST are generally smaller in magnitude than those for T2m. These results are consistent with previous studies comparing LST and T2m anomalies. In addition, a general increase in *r* with latitude is observed for comparisons with the IR datasets, but not for the multisensor MW dataset, which appear to be less variable across different latitudes (not shown). Furthermore, the distribution of MW anomalies appears to match that for T2m more closely than for the IR datasets (Figure 2-1). This suggests that MW LST anomalies might provide a better proxy for T2m anomalies than those from IR LST

datasets. This may be due to the larger and more spatially representative footprint of the MW LST dataset and the effects of cloud contamination in the IR LST datasets, which does not affect the MW LSTs.

Table 2-2: Median correlation coefficient (r) and LST vs. T2m slope (m) from all available stations for each LST_cci dataset comparison.

Comparison Type		MODIS/ Aqua	MODIS/ Terra	ATSR-2	AATSR	Multisensor IR	Multisensor MW
T_{min}	r	0.62	0.57	0.60	0.63	0.70	0.73
	m (K/K)	0.71	0.63	0.56	0.61	0.67	0.70
T_{max}	r	0.77	0.78	0.74	0.80	0.78	0.79
	m (K/K)	0.91	0.90	0.90	0.89	0.78	0.80
T_{mean}	r	0.78	0.80	0.67	0.72	0.84	0.84
	m (K/K)	0.85	0.88	0.87	0.86	0.79	0.85
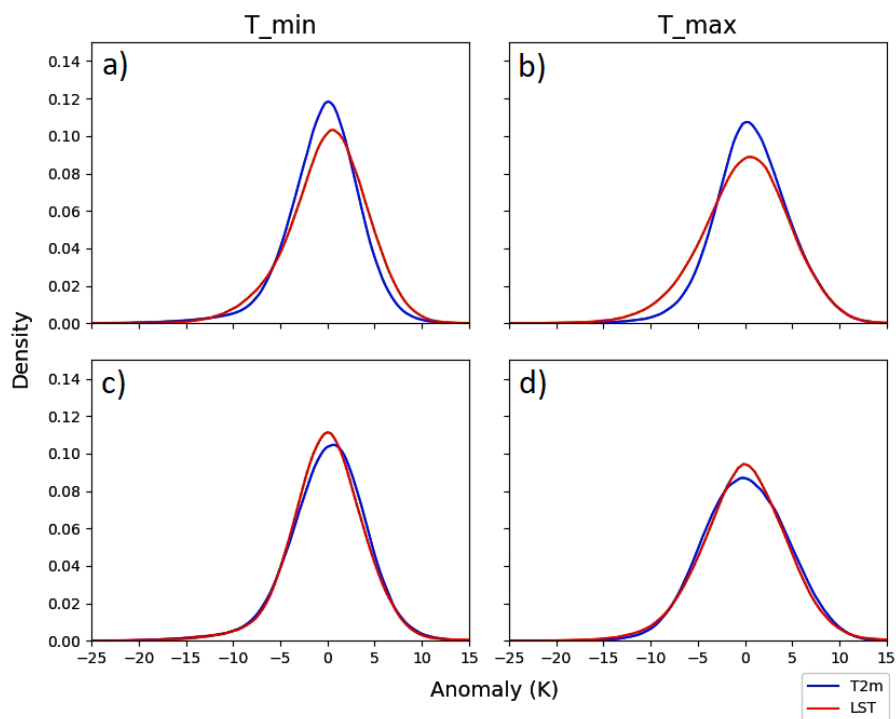
Figure 2-1: Probability density functions for all daily anomalies for a) AQUA_MODIS_L3C LST$_{night}$ and T$_{min}$, b) AQUA_MODIS_L3C LST$_{day}$ and T$_{max}$, c) the SSMI_SSMIS_L3C LST$_{desc}$ and T$_{min}$, and d) the SSMI_SSMIS_L3C LST$_{asc}$ and T$_{max}$. Blue: T2m. Red: LST

Having established a strong relationship between LST and T2m anomalies, the stability of the LST datasets is assessed by calculating the trend in the time series of monthly LST-minus-T2m anomalies averaged over the whole study region. As the T2m data are homogenised, a statistically significant trend in this LST-T2m difference is assumed to indicate that the LST dataset is inhomogeneous. This is found to be the case for the MULTISENSOR_IRCDR_L3S (LST$_{night}$) (Figure 2-2), SSMI_SSMIS_L3C dataset (LST$_{desc}$ and LST$_{mean}$) (Figure 2-3), TERRA_MODIS_L3C (LST$_{night}$, LST$_{mean}$) and ERS-2_ATSR__L3C (LST$_{day}$, LST$_{mean}$) (Figure 2-4). These
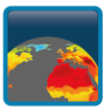
datasets are therefore considered inhomogeneous and unsuitable for use for robust climate trend analysis. However, it should be noted that the time series for the individual sensors SSMI and SSMI/S that comprise the SSMI_SSMIS_L3C data set, and the ATSR-2 and AATSR that comprise the MULTISENSOR_IRCDR_L3S dataset appear temporally stable. Of the six LST_cci datasets assessed here, only the AQUA_MODIS_L3C and ENVISAT_ATSR__L3C datasets appear free from non-climatic discontinuities (Figure 2-4) based on the approach to assess the stability of the LST_cci datasets that has been adopted in this study.

Trends in LST and equivalent T2m data are calculated for the two datasets considered temporally stable. For AQUA_MODIS_L3C, significant trends in LST of 0.64-0.66 K/decade are obtained, which compare well with the equivalent T2m trends of 0.52-0.59 K/decade; no statistically significant difference is found between these trends in LST and T2m. The trends for ENVISAT_ATSR__L3C are found to be statistically insignificant, which is due to the specific years available for the analysis. This is demonstrated through a comparison of trends for T2m for the AQUA_MODIS_L3C and TERRA_MODIS_L3C time periods, where the addition of just two additional years of data at the beginning of the TERRA_MODIS_L3C period (2000-2001) is found to reduce the trends in T2m by ~0.2 K/decade. This highlights the importance of using a long and homogeneous time series of data to calculate climate trends.

The results of this study also demonstrate that the method used to compare LST and T2m data can affect results. The IR satellite LST data are only available for cloud-free conditions but excluding cloudy T2m observations by temporally matching the LST and T2m observations introduces an artefact into the comparison as shown by Figure 2-5. This results in more negative anomalies in T2m during winter months and more positive anomalies during summer months, leading to an annual cycle and non-zero mean difference in the LST-minus-T2m anomaly time series for the IR datasets (e.g. Figure 2-4). This is not present in the SSMI_SSMIS_L3C comparison, which is all-sky, and is removed in the IR comparisons when the T2m anomaly time series is regenerated from 'all-sky' T2m observations (not shown). Nevertheless, when the trends in T2m are recalculated from the 'all-sky' T2m data, they are still statistically significant and almost identical (0.01-0.06 K/decade difference) for the AQUA_MODIS_L3C analysis. A more substantial change in the T2m trends is found for the ENVISAT_ATSR__L3C analysis when all-sky T2m data are used, however these trends are all found to be statistically insignificant. Therefore, it is concluded that the results presented in this study do not offer any evidence that a clear-sky bias affects trends calculated using cloud-free IR observations.

2.1.2.4 Conclusions

In general, the collocated LST vs T2m station anomalies show reasonable correlations and slopes (r and m ≈ 0.6-0.9), which is a positive result in terms of the quality of LST_cci datasets and for the use of LST to complement T2m analyses in climate applications. The multisensor IR and MW products show non-climatic discontinuities at sensor transitions that need to be addressed to enable these data to be used for trend analysis. However, the stability of the individual sensors comprising these datasets is encouraging. The TERRA_MODIS_L3C and ERS-2_ATSR__L3C datasets also appear to be inhomogeneous and a visible drift with time is observed for TERRA_MODIS_L3C. Terra MODIS does suffer from orbital drift at the start of its lifetime, and this will be analysed in Phase-2 by the LST_cci Science Team. For the two LST_cci datasets assessed here that are considered free from non-climatic discontinuities, AQUA_MODIS_L3C and ENVISAT_ATSR__L3C, the trends for LST and T2m are not statistically significantly

different. This suggests these LST_cci datasets can reliably be used for trend analysis and to augment the analysis of T2m.

2.1.3   Feedback on scientific utility of the LST_cci products

Generally, the LST_cci products have been easy to use, with a well described netCDF format. However there are some discrepancies in the format between the IR and MW products that makes analysis that uses both these types of products more challenging. The first is the difference in classification of day and night for IR data, and ascending and descending for MW data. This adds additional processing to read in the data when working with both data types. Secondly the two data types contain different variables in the files: a quality flag ('qual_flag') is provided with MW data but not IR data. The IR data is provided with a land water mask ('lwm') and number of cloudy pixels ('ncld') instead. The IR data also comes with the land cover class ('lcc') whilst the MW data does not. Whilst there is some sense to the differences, quality flags would certainly be useful with all data products, as would the land cover class and land water mask. Understandably the use of number of cloudy pixels is different for IR and MW data. The more consistent the format can be between products the easier they are to use in analyses.

In the MULTISENSOR_IRCDR_L3S product, some data files were found to have incorrect global attribute 'platform': for ATSR_3 the platform should be Envisat, but is given as ERS-2, which can be identified by the purple dashed line in Figure 2-2. For the MODIS v1.0 products (and possibly other products), the 'standard_name' field contents for both latitude and longitude is set to 'latitude'. This has been corrected in v2.0 products.

Some anomalously low temperatures were identified, particularly in the MODIS datasets, which are thought to be due to cloud contamination. Whilst there are only a few there is no easy way to mask these values out during processing. It would be useful to have some guidance and further information on how best to handle this problem.

When originally performing this analysis using v1.0 products, it was found that IR products became 'noisier' with increasing latitude compared to T2m observations, reflected in the lower LST vs T2m correlations and slopes. This was not observed in the MW product and was attributed to a difference in the way observations are averaged over a grid cell. For the IR v1.0 products, the grid cell value can be an average value from multiple orbits, whereas the MW product uses only the observation closest in time to the nominal overpass time of the sensor. This was changed for the IR v2.0 products used in this updated study report, resulting in a significant reduction in the observed 'noise', although the MULTISENSOR_IRCDR_L3S product used here is v1.0, as v2.0 was not available in time for this study.

Finally, non-climatic discontinuities are evident in four of the six LST_cci datasets assessed in this study. In particular, the multisensor products have discontinuities where there is a change in sensor. It is very strongly recommended that these discontinuities are addressed in future versions of the dataset so that they can be used for climate applications that require temporally stable datasets.
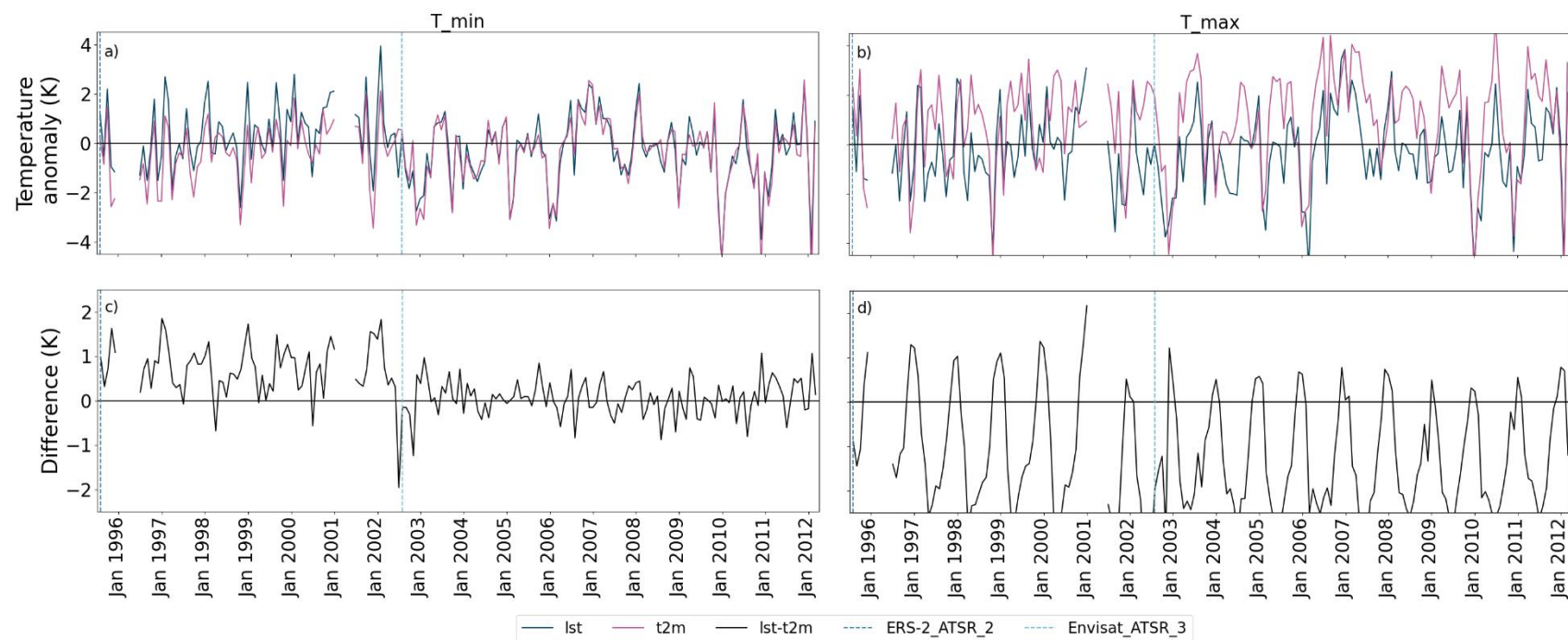
Figure 2-2: Monthly mean (a) LST$_{night}$ and T$_{min}$ and (b) LST$_{day}$ and T$_{max}$ anomaly (K, relative to 1996-2012) averaged over all available stations for the MULTISENSOR_IRCDR_L3S dataset, with the respective differences in the time series shown in (c) and (d). The change in sensor from ATSR-2 (early period) to AATSR (later period) is shown by the vertical blue line in each panel.

T_min   **T_max**
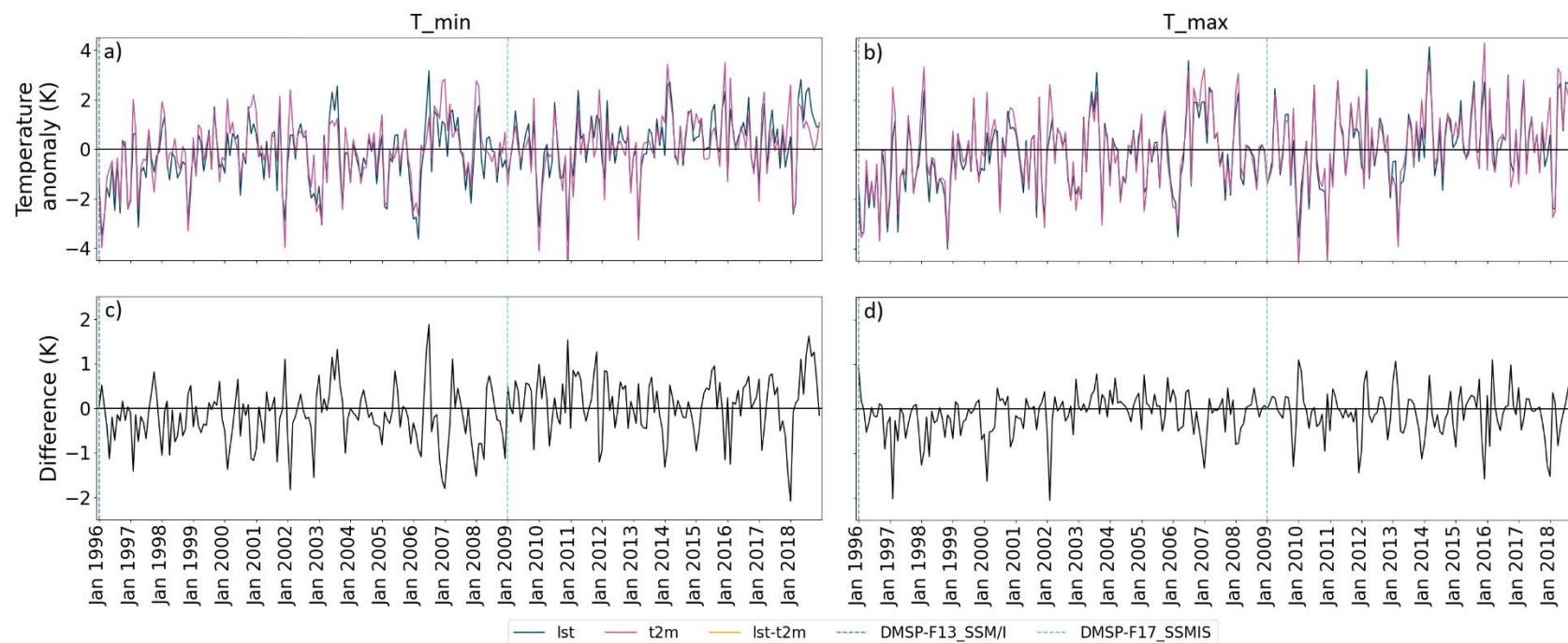
Figure 2-3: As for Figure 2-2 but for the SSMI_SSMIS_L3C dataset. Monthly mean (a) LST$_{night}$ and T$_{min}$ and (b) LST$_{day}$ and T$_{max}$ anomaly (K, relative to 1996-2018) averaged over all available stations for the SSMI_SSMIS_L3C dataset, with the respective differences in the time series shown in (c) and (d). The change in sensor from SSMI (early period) to SSMI/S (later period) is shown by the vertical blue line in each panel.
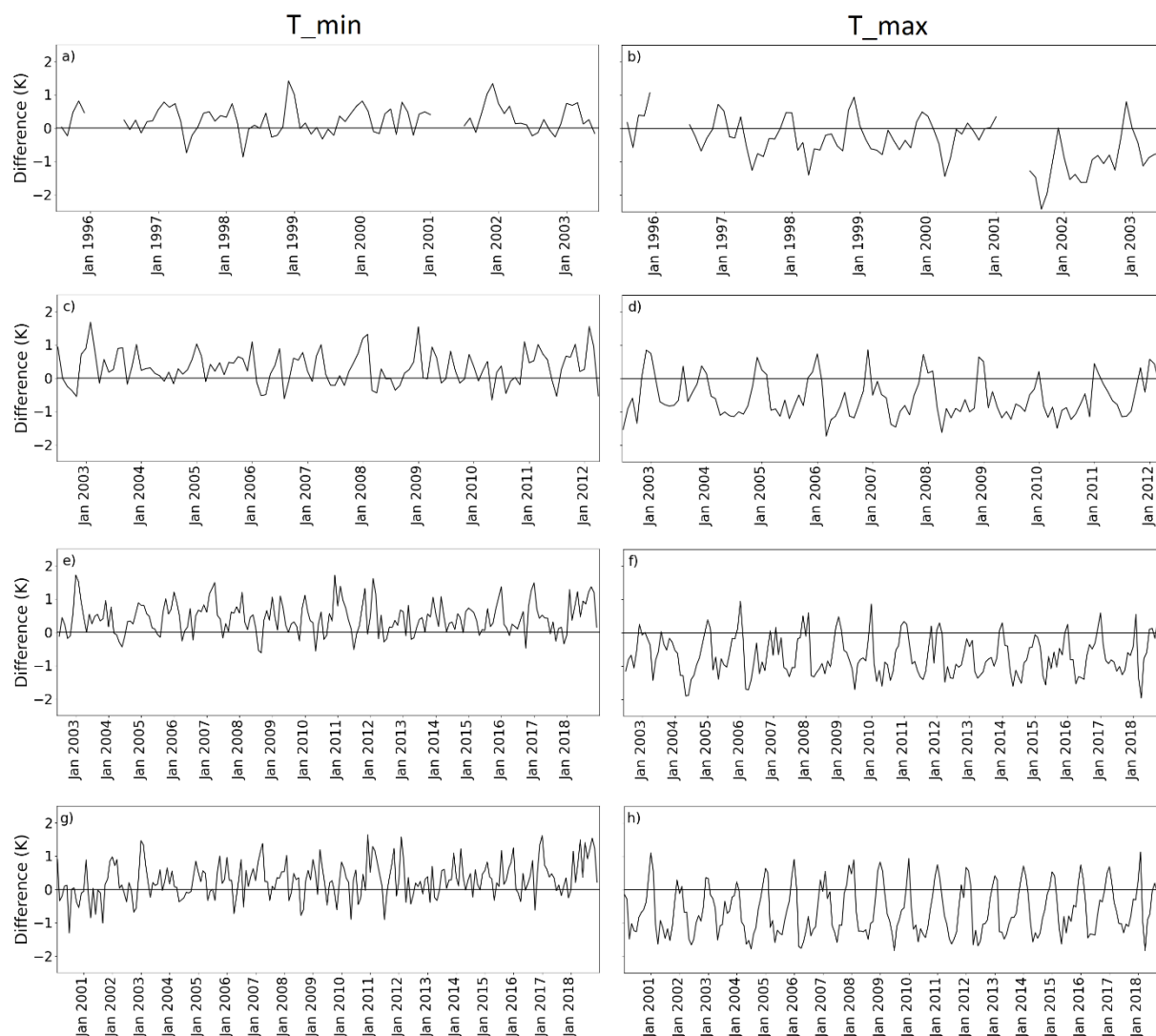
Figure 2-4: LST-minus-T2m monthly anomaly time series for a) ATSR-2 Tmin, b) ATSR-2 Tmax, c) AATSR Tmin, d) AATSR Tmax, e) MODIS/Aqua Tmin, f) MODIS/Aqua Tmax, g) MODIS/Terra Tmin, and h) MODIS/Terra Tmax comparisons
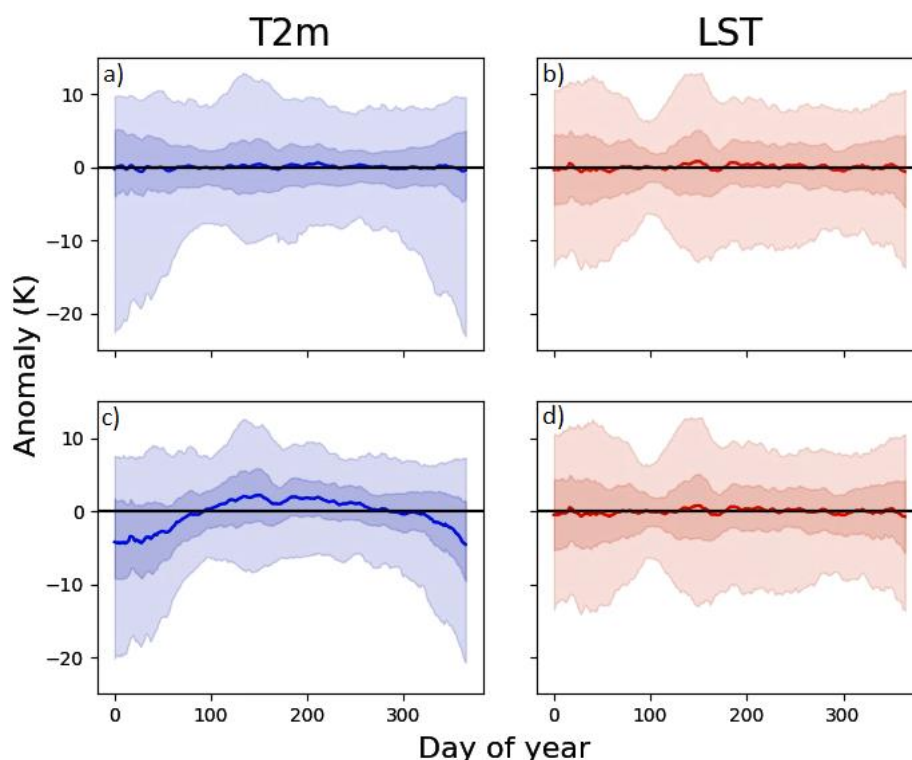
Figure 2-5: Percentiles of daily anomalies (K) for each day of the year averaged over five stations above 60°N for Tmax (left) and LSTday (right) before temporal matching between the T2m and LST data is performed (upper), and after temporal matching is performed (lower). The solid line shows the mean, darker shading the inter-quartile range, and lighter shading the full range of data. The percentiles have been smoothed over a 21-day moving window using a convolution function to improve the visual clarity of the plot. Data are from the TERRA_MODIS_L3C comparison

2.2 Construction of a gap-free multisensor ice surface temperature product for the Greenland ice cap and assimilation into atmosphere and ice sheet models (DMI)

2.2.1 Key Messages

❖ High resolution Level 2 v1.0 LST_cci products (ENVISAT_ATSR__L2P, AQUA_MODIS_L2P, TERRA_MODIS_L2P) of Ice surface temperature (IST) from the Greenland ice sheet are used to construct a daily gap free level 4 Ice surface temperature product.

❖ Data are evaluated against observations on the ice sheet and assimilated into a surface mass budget model of snow and firn processes for one year (2012).

❖ The resulting L4 product performs satisfactorily in terms of quality when compared with surface temperature from IceBridge.

2.2.2 Scientific Analysis

2.2.2.1 Aims of the study

The aim of this study is to assess the use of satellite LST data products for improving model hindcasts of Greenland ice sheet surface mass budget. This requires that the high-resolution Level 2 LST_cci products of Ice surface temperature (IST) from the Greenland ice sheet are validated and used to construct a daily gap free level 4 IST product. As a pilot, the data products for the year 2012 were assessed for use in combination with a regional climate model (RCM) and surface mass balance (SMB) model. For the pilot year, the performance of the RCM HIRHAM5 in calculating the surface energy budget over the Greenland ice sheet and determining the extent of surface melt will be assessed. The LST data will also be integrated into a snow and firn (snow that has survived at least one annual cycle) SMB and run offline to assess the impact of including observational data to improve simulations of melt and retention. The protocol established in the Retention model inter-comparison project (RetMIP) [RD-04] for evaluating improvements in the model system with data assimilation is adopted in this study.

The year 2012 has been chosen for this project. This was a year in which extensive surface melt covered most of the ice sheet, an event that occurred for the first time in the direct observational record. This was an important year with the lowest surface mass budget then in the record, but also a challenging one for climate models, many of which underestimated the contribution to melting of turbulent heat fluxes, especially the sensible heat flux [RD-05].

2.2.2.2 Data and Method

Due to the high latitudes of the Greenland ice sheets, it is not feasible to use aggregated day/night observations from ascending and descending orbits. Therefore, a special data package was made available for this UCS from the LST_cci project, consisting of the L2 1 km satellite IST observations from AATSR and MODIS. In addition, IST observations from the AASTI (Arctic and Antarctic ice Surface Temperatures from thermal Infrared satellite sensors) AVHRR GAC v2 data set provided by DMI and MET.NO, have been included in the analysis [RD-06]. The data satellite products used in this study are listed in Table 2-3. The level 3 data fields are aggregated to daily using a similar statistical methodology as in Høyer et al., (2016) [RD-07] to generate daily, gap-free estimates of the ice surface temperature for the Greenland Ice Sheet with a 0.01° longitude and 0.02 latitude resolution (L4 Optimal Interpolation).

Table 2-3: List of LST data sets used in the study

Product String and Version	Sensor type	Resolution	Data availability
ENVISAT_ATSR__L2P v1.0	IR	1 km swath	Jan-April, 2012
TERRA_MODIS_L2P v1.0	IR	1 km swath	Jan-Dec, 2012
AQUA_MODIS_L2P v1.0	IR	1 km swath	Jan-Dec, 2012
AASTI AVHRR GAC v2.0	IR	4 km swath	Jan-Dec, 2012

Thermal infrared satellites observe the skin of the snow and ice surface, which can deviate substantially from e.g. a T2m observation [RD-08, RD-09]. For a proper validation of the satellite products, it is therefore

important to compare against the radiometric surface temperature. These types of observations are available from the Operation IceBridge project [RD-10], which conducted flight campaigns, carrying a thermal infrared radiometer. Airborne radiometric surface temperature observations were used to tune the statistical processing (e.g. temporal averaging window) and to determine the quality of the different satellite products both in terms of spatial variability and any offsets.

2In parallel to the L4 data production, an LST_cci specific model run was carried out without additional data to use as control against the assimilated version. Six hourly forcing data from the RCM is used to drive the SMB model where surface energy balance variables are used to calculate the ice surface temperature and melt potential. When melt occurs, the model calculates the retention of liquid meltwater and refreezing within the snowpack and deeper firn layers. The sum of precipitation and runoff of meltwater gives the daily surface mass budget over the ice sheet. The SMB model is described in full in Langen et al. (2014, 2018) [RD-11, RD-12] and the RCM set up is described in Mottram et al. (2017) [RD-13]. The schematic diagram in Figure 2-6 shows how SMB is calculated.

In this study, the quality of the modelled LST in the control run is assessed through a comparison with the LST_cci data. Subsequent runs assimilate the LST_cci data in the SMB model via the LST variable (which is referred to here as IST). As the IST is calculated at six hourly intervals in the model and daily in the dataset, an interpolation routine is applied to simulate the daily cycle before adding values to the input data set driving the model. To avoid model instabilities, the observed IST is statistically weighted with the modelled IST before calculating the potential production of melt water and temperature in the snowpack. Finally, the daily SMB is calculated and compared with the control run and observations from PROMICE weather stations.
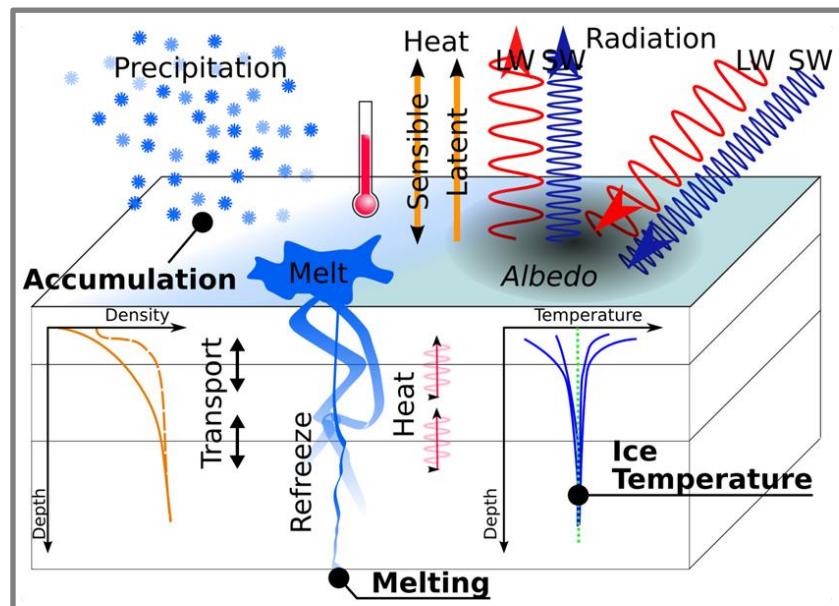
Figure 2-6: Schematic diagram showing the SMB calculation from RCM output. (image credit: Christian Rodehacke, DMI)

2.2.2.3 Results

An example of the different satellite products is shown in Figure 2-7, where the various sampling skills of the L3 products are evident. (A)ATSR sampling is limited compared to MODIS and AASTI L3. The difference in the range of IST can also be noted with AASTI and the L4 OI being warmer compared to MODIS and (A)ASTI.
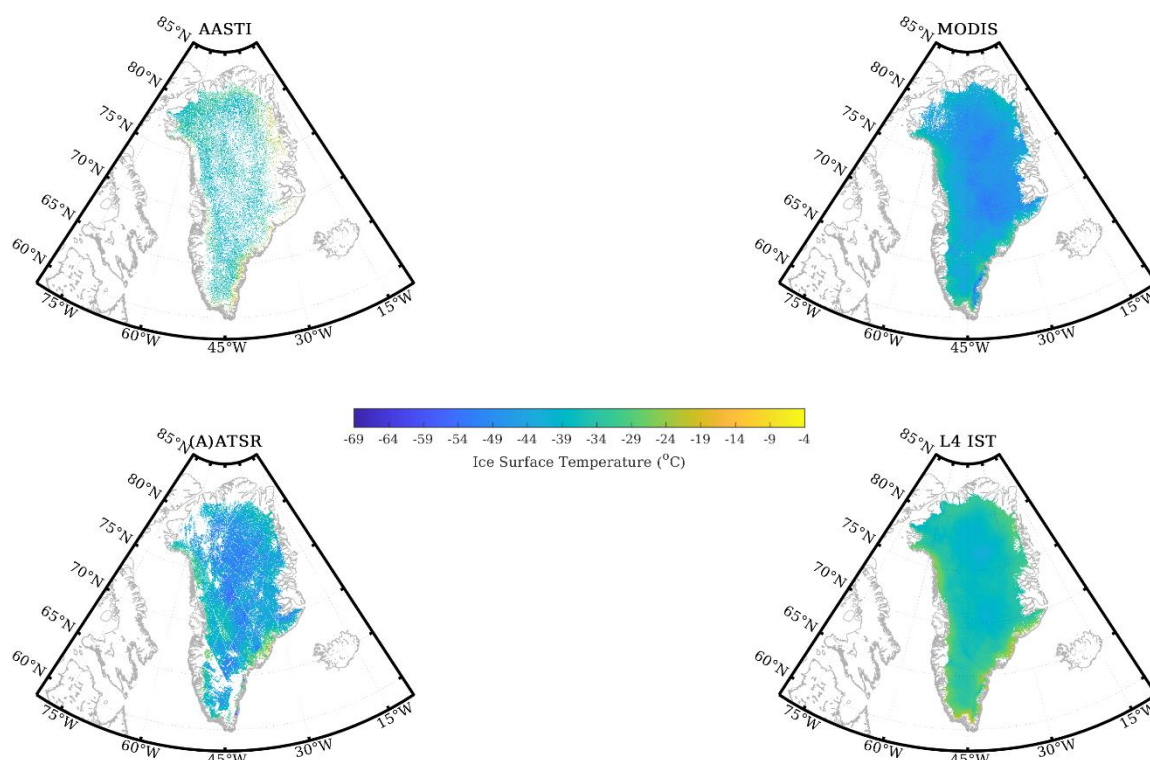
Figure 2-7: Examples of aggregated IST observations from Jan 9th, 2012 over the Greenland Ice Sheet. Top row is Level 3 AASTI GAC (left), Level 3 MODIS Aqua and Terra (right) and bottom row is Level 3 AATSR (left) and Level 4 Optimal Interpolation based on all three input data sets (right).

Time-series of mean daily IST values of the Greenland Ice Sheet and their associated standard deviation from the L3 AASTI, L3 MODIS, L3 AATSR and L4 OI IST are shown in Figure 2-8. Note that the (A)ATSR dataset ends on 9th April 2012 due to loss of contact with the ENVISAT platform. Due to the previously mentioned sampling issue and the limited length of data (only part of the study year 2012 is available), (A)ATSR data were not used to generate the final Level 4 IST product. The MODIS mean daily IST (green) in 2012 is significantly colder compared to the AASTI (purple) and L4 OI (blue) products.
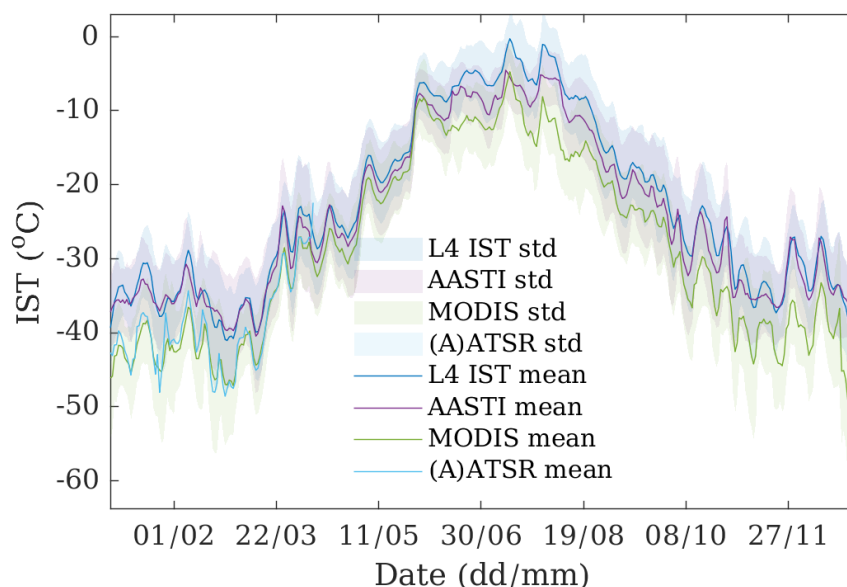
Figure 2-8: Daily mean IST (solid lines) and its standard deviation (shaded area) in 2012 from the L3 AASTI (purple), MODIS (green), AATSR (cyan) and L4 OI (blue).

The monthly mean IST and its standard deviation over the Greenland Ice Sheet from the different L3 products and the L4 OI IST is shown in Figure 2-9. Besides the annual cycle of warming during the summer period, the monthly means of the L4 OI product agree better with AASTI than MODIS, which is consistently colder than the other datasets and has higher standard deviation for most of the months.
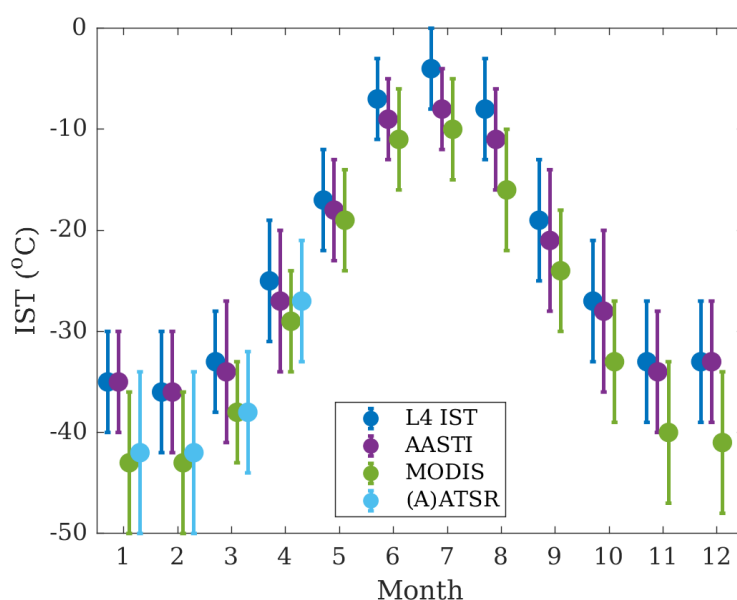
Figure 2-9: Monthly mean IST (dots) and standard deviation (vertical bars) from the L3 AASTI (purple), MODIS (green), AATSR (cyan) and L4 OI (blue).

Figure 2-10 shows two examples of the L3 MODIS and AASTI products from May 8th 2012, compared against Icebridge observations. The aggregated MODIS observations are cold compared to the IceBridge

observations, which has also been reported in the literature for NASA MODIS products, whereas the agreement is better for the AASTI AVHRR GAC data. Nonetheless, the pixel-to-pixel variability in the aggregated MODIS observations is smaller (e.g. lower standard deviation) than in the AASTI observations, probably due to the better coverage. These examples are representative for the other IceBridge comparisons and therefore a dynamical bias correction was implemented for the MODIS LST_cci products using the AASTI GAC data [RD-14] when combining the L3 products into a level 4 product.
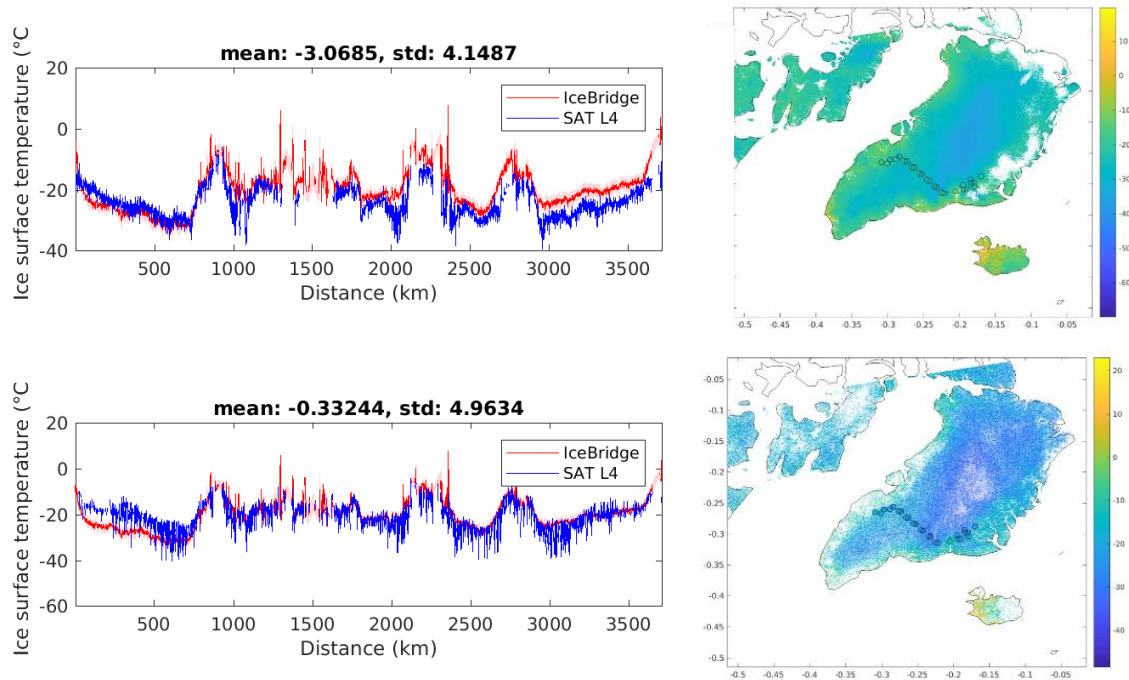
Figure 2-10: Validation of MODIS (top) and AASTI (bottom) level 3 IST products against IceBridge observations from May 8th, 2012. Left figures show along track surface temperature observations and right figures show aggregated satellite IST fields from the day with overlaid IceBridge observations (circles).

An example of the resulting L4 product is shown in Figure 2-11 (right), where the IceBridge flight points are marked as circles. The comparison against surface temperature from IceBridge (left) shows that the L4 product performs satisfactorily in terms of quality.
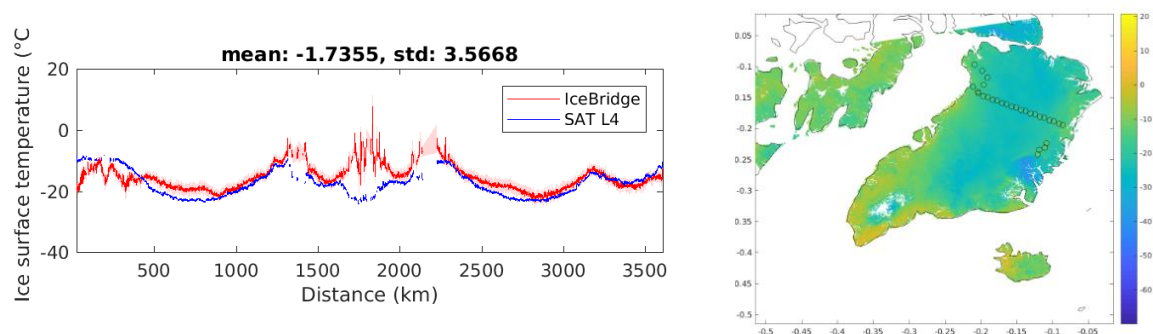
Figure 2-11: Left - example of Level 4 IST observations (blue) compared against IceBridge observations (red). Right – example of L4 product with IceBridge flight points marked as circles.

The daily level 4 fields provide the input for the modelling analysis. Model simulation experiments and sensitivity studies are still ongoing at the time of writing.

2.2.2.4 Conclusions

LST_cci L2 MODIS Aqua/Terra v1.0 data have been used together with AVHRR data (sourced outside of LST_cci) to create daily L4 IST data for Greenland. Analysis against airborne IST observations suggests that the LST_cci MODIS data may be cold biased by several K. The equivalent AVHRR data do not exhibit such a cold bias. However, the variance of the agreement between MODIS and the airborne IST observations is found to be lower than for the equivalent AVHRR data. After implementing a bias-correction to the MODIS data, the agreement between the derived L4 IST data and airborne IST data is found to be satisfactory.

These L4 data will be ingested into an SMB model, which is driven by RCM output, to estimate ice melt and retention. The impact of using observed IST data in the model will be assessed by comparing modelled and observed estimates of these parameters for the extreme melt event of 2012.

2.2.3 Feedback on scientific utility of the LST_cci products

The LST_cci products were very easy to use in this study. It is appreciated that a special data delivery was set up for this project to deliver Level 2 swath observations. For high latitude regions, it is not feasible to divide products into ascending and descending due to the larger number of overpasses compared with lower latitudes, but the level 2 data worked very well. The use of the data was very easy due to the same file formatting and naming conventions across the different sensors.

The scientific quality of the v1.0 products used in this study appears to be an area where improvements could be made in the future. The validation showed a general cold offset of a few K of the MODIS products, compared to IceBridge observations, but there were also regions where 30-40 K offset were visible that do not look like typical cloud contamination. Such discrepancies are very large and could be examined in more detail in future algorithm improvements. In general, it is suggested that dedicated IST algorithm improvements could be carried out in order to improve both on the offset and on the large regional errors presented in this study. This study uses v1.0 LST_cci products and significant modifications have been made to the MODIS LST_cci v2.0 products that may improve the quality of these data including a new enhanced probabilistic cloud detection algorithm. However, as these v2.0 level 2 data were not available in time for this study, these improvements have not yet been assessed.

2.3 Urban Case Study: A global investigation of Surface Urban Heat Islands (RUB)

2.3.1 Key Messages

- ❖ Surface Urban Heat Island (SUHI) Intensity (SUHII) estimates derived from three 0.01° LST_cci v1.0 custom products (TERRA_MODIS_L3C, ERS-2_ATSR_L3C, ENVISAT_ATSR_L3C) are consistent in terms of peak time.

❖ The SUHII magnitude of the TERRA_MODIS_L3C 0.01° v1.0 data is slightly higher than that of the ERS-2_ATSR_L3C 0.01° v1.0 and ENVISAT_ATSR_L3C 0.01° v1.0 data products.

❖ The AQUA_MODIS_L3C 0.01° v1.0 data have not been used in this analysis due to problems with cloud masking.

❖ The SUHII estimates and hysteretic cycles calculated from the 0.01° LST_cci custom products agree with the published literature.

❖ The Land Cover Class (LCC) data included in each LST_cci netCDF file need to be updated to reflect Land Cover (LC) changes.

2.3.2 Scientific Analysis

2.3.2.1 Aims of the study

The Urban Heat Island (UHI) refers to the relative warmth of urban areas compared to their surrounding rural areas and is the most studied urban climate effect. It is a direct result of urbanization and is driven primarily by the conversion of natural surfaces to impervious surfaces. The intensity of the Surface UHI (SUHII), which is the difference between urban and rural LST, exhibits seasonal hysteretic cycles (i.e., looping patterns), the shape and direction of which vary across climate zones. For instance, in wet climates, SUHII peaks during the summer and is positive throughout the year, while in dry climates it peaks in spring and is negative during summer and autumn [RD-15, RD-16]. These looping patterns are the result of time lags between the energy and water budget of cities and that of rural areas.

The aim of this case study is to investigate the use of the 0.01° LST_cci custom products for estimating SUHIIs and for characterizing their temporal behaviour. To achieve this objective, this work uses 24 years (1995 - 2018) of daily day- and night-time LST data over the most densely populated regions of the world and calculates the daily (day- and night-time) SUHII of each city. The overall goal is to analyse these estimates with respect to climate.

2.3.2.2 Data and Method

The LST_cci data used in this case study are the ERS-2_ATSR_L3C 0.01° v1.0, ENVISAT_ATSR_L3C 0.01° v1.0, and TERRA_MODIS_L3C 0.01° v1.0 IR data products. The sensing time and the data availability of each product are given in Table 2-4, while the regions of interest of the employed data are presented in Figure 2-12. The selected regions (25 in total) include the most populated areas in every continent and major climate zones of the world.

To identify and delineate the cities included in each focus region (Figure 2-12), information from the ESA CCI Land Cover (LC_cci) product is used. The LC_cci product provides global land cover (LC) maps at 300 m that are available annually starting from 1992. In this work the annual LC data are resampled to the LST_cci 0.01° × 0.01° grid, by calculating the LC class (LCC) fractions of each grid cell. Then, a binary mask of all the grid cells that have an urban fraction greater than or equal to 95% and a water fraction equal to 0% is created for every year between 1995 and 2018. To eliminate single pixels and small objects from the resulting masks, a morphological operator that removes any objects with eight or less connected pixels is applied. The filtered masks are then segmented into clusters that represent cities and labelled with a

unique ID. To ensure consistency through the years, the same unique label is given to all the instances of each city.

Table 2-4: A summary of the LST_cci products used in the study.

Product String and version	Sensor type	Resolution	Data availability	Local overpass time
ERS-2_ATSR__L3C 0.01° v1.0	IR	0.01°	August 1995 – June 2003	10:30 am / pm
ENVISAT_ATSR__L3C 0.01° v1.0	IR	0.01°	July 2002 – April 2012	10:00 am / pm
TERRA_MODIS_L3C 0.01° v1.0	IR	0.01°	February 2000 – December 2018	10:30 am / pm
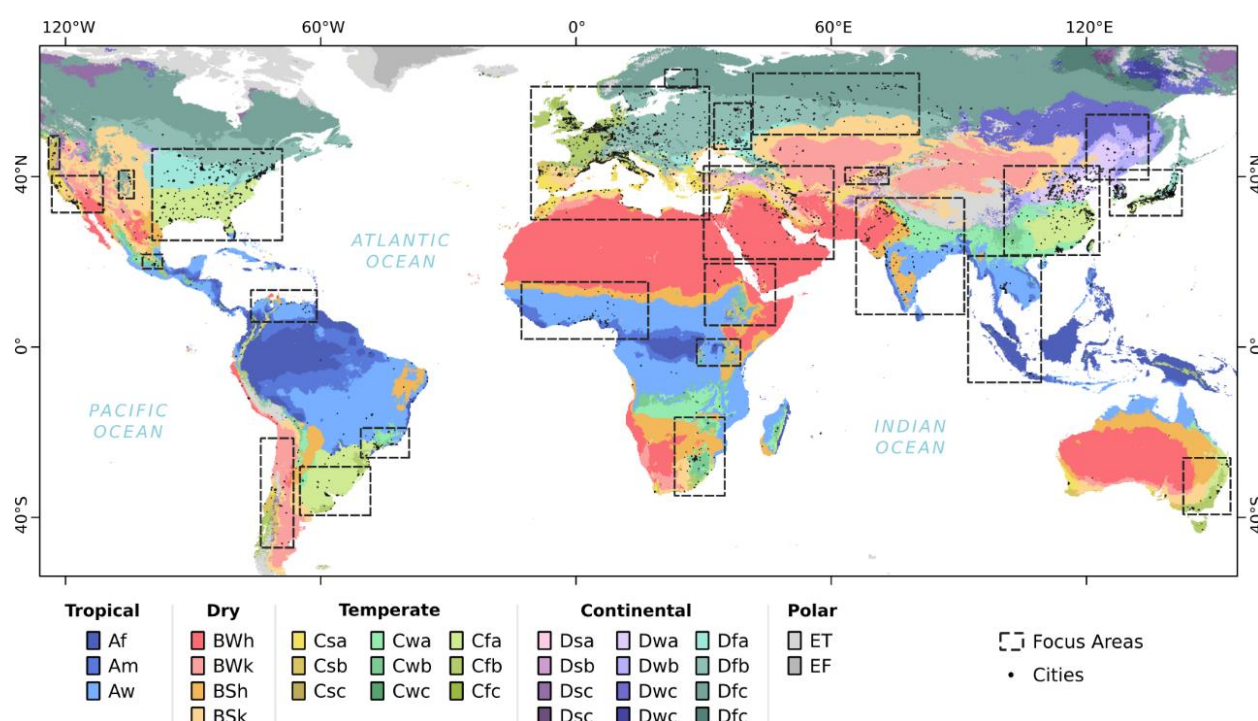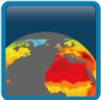
Figure 2-12: The regions of interest for LST data used in this study. The colours indicate the Köppen-Geiger climate zone.

For the identified cities, masks that delineate all the natural grid cells that are appropriate for calculating the SUHII are also created. This is done using the algorithm proposed in [RD-16], which creates and expands a buffer around each city until its size is approximately that of the urban area. To ensure consistency in the SUHII estimates over the years, a single rural mask, representative for all the years between 1995 and 2018, is created for each city. This is achieved by selecting only the buffer grid cells that comply with the following criteria:

❖ the rural LCC fraction is ≥95% for every year between 1995 and 2018;

❖ the urban and water LCC fractions are equal to 0% for every year between 1995 and 2018, and

❖ the grid cell elevation does not differ by more than +/- 200 m from the median elevation of the corresponding city.

The urban and rural masks are then used to calculate the urban and rural daily LST means for each city. This is done separately for the day- and night-time LST, and for each LST_cci data product used in this case study (Table 2-4). To ensure the calculation of reliable means, only grid cells where the LST value is between 240 K to 350 K and the LST total uncertainty is below or equal to 2 K are used. In addition to these two tests, a Median-Absolute-Deviation outlier test is also used to remove any remaining outliers, for example, due to cloud contamination (the test's statistics are calculated from all the available LST data for each city, product, and year separately). The daily SUHIIs for each city are then calculated as the difference between the daily urban and rural LST means as shown in Equation 2-14. This is done separately for the day- and night-time data and for each one of the three 0.01° LST_cci data products utilized in this work.

$$\textbf{Equation 2-14} \quad SUHII = \overline{LST}_{urban} - \overline{LST}_{rural}$$

The SUHII data are finally used to derive a climatology for each densely populated Köppen-Geiger climate zone and for calculating the corresponding daytime and night-time SUHII hysteretic cycles. To mitigate the influence of cloud gaps in these calculations, only SUHII estimates where at least 70% of the urban and rural grid cells are available are used.

2.3.2.3 Results

Using the proposed method, 1,588 cities in 12 climate zones have been delineated, namely: tropical savanna (Aw), hot desert (BWh), hot semi-arid (BSh), cold semi-arid (BSk), hot-summer Mediterranean (Csa), humid subtropical (Cfa), oceanic (Cfb), dry-winter humid subtropical (Cwa), dry-winter subtropical highland (Cwb), hot-summer humid continental (Dfa), warm-summer Humid Continental (Dfb), and monsoon-influenced hot-summer humid continental (Dwa). From these 12 climate zones, 11 contain more than 50 cities, six more than 100 cities, and one more than 300 cities. Figure 2-13 presents the location and the number of cities per climate zone, and the corresponding daytime (~10:30 local time) and night-time (~22:30 local time) SUHII climatologies, derived as the bivariate distribution of daily SUHII and rural LST (i.e. the $\overline{LST}_{rural}$). The derived climatologies are most different in daytime. The shape of the Aw SUHII daytime climatology approximates that of a concave blob, which is attributed to the weak seasonality of tropical climates. The shape of the semi-arid (BSh, BSk) and hot mediterranean (Csa) daytime climatologies is more complex than that of Aw and clearly influenced by seasons. The BSh, BSk and Csa SUHIIs are mostly negative and become minimum when $\overline{LST}_{rural}$ peaks. The Cwa and Cwb daytime climatologies also differ considerably, with Cwb exhibiting a more pronounced SUHII seasonality that is negative when $\overline{LST}_{rural}$ is maximum. Finally, in the humid temperate (Cfa and Cfb) and continental (Dfa, Dfb and Dwa) climates the daytime SUHII is mostly positive and generally in sync with the rural LST (except for Dfa, Dfb and Dwa when $\overline{LST}_{rural}$ is ≤300 K). In contrast to the daytime results, the night-time climatologies for all climate zones are rather flat and almost always positive.

Figure 2-14 presents the corresponding daytime and night-time hysteretic cycles for each one of the examined climate zones using TERRA_MODIS_L3C; results for ERS-2_ATSR_L3C and ENVISAT_ATSR_L3C are similar (not shown). These hysteretic cycles essentially represent the time series of climatological monthly mean SUHII vs $\overline{LST}_{rural}$. In climates with pronounced seasons, the daytime cycles are particularly elongated along the y-axis (i.e., the LST rural dimension), while in climates with weak seasonality they are more symmetrical. In wet climates (e.g. Cfa, Cfb and Dfa) the daytime cycles show a clear concave-up

pattern, as the model of Manoli et al. [RD-15] suggests. In dry climates, the concave-down pattern is clear only in Csa. In BSh the mean cycle exhibits a twisted shape, while in BSk, a great variety of individual hysteretic cycles are observed (exhibiting concave-up, - down, flat, and twisted patterns; not shown) that are not well represented by the mean. The hysteretic cycle with the greatest daytime SUHII range is Dwa (5.2 K), followed by Cwb (4.1 K) and Dfa (3.5 K), while the ones with the smallest range are BSk (0.8 K), and BSh (0.8 K). The direction of the daytime cycles is clockwise in most cases. The night-time hysteretic cycles are all very similar and quite featureless (Figure 2-14).
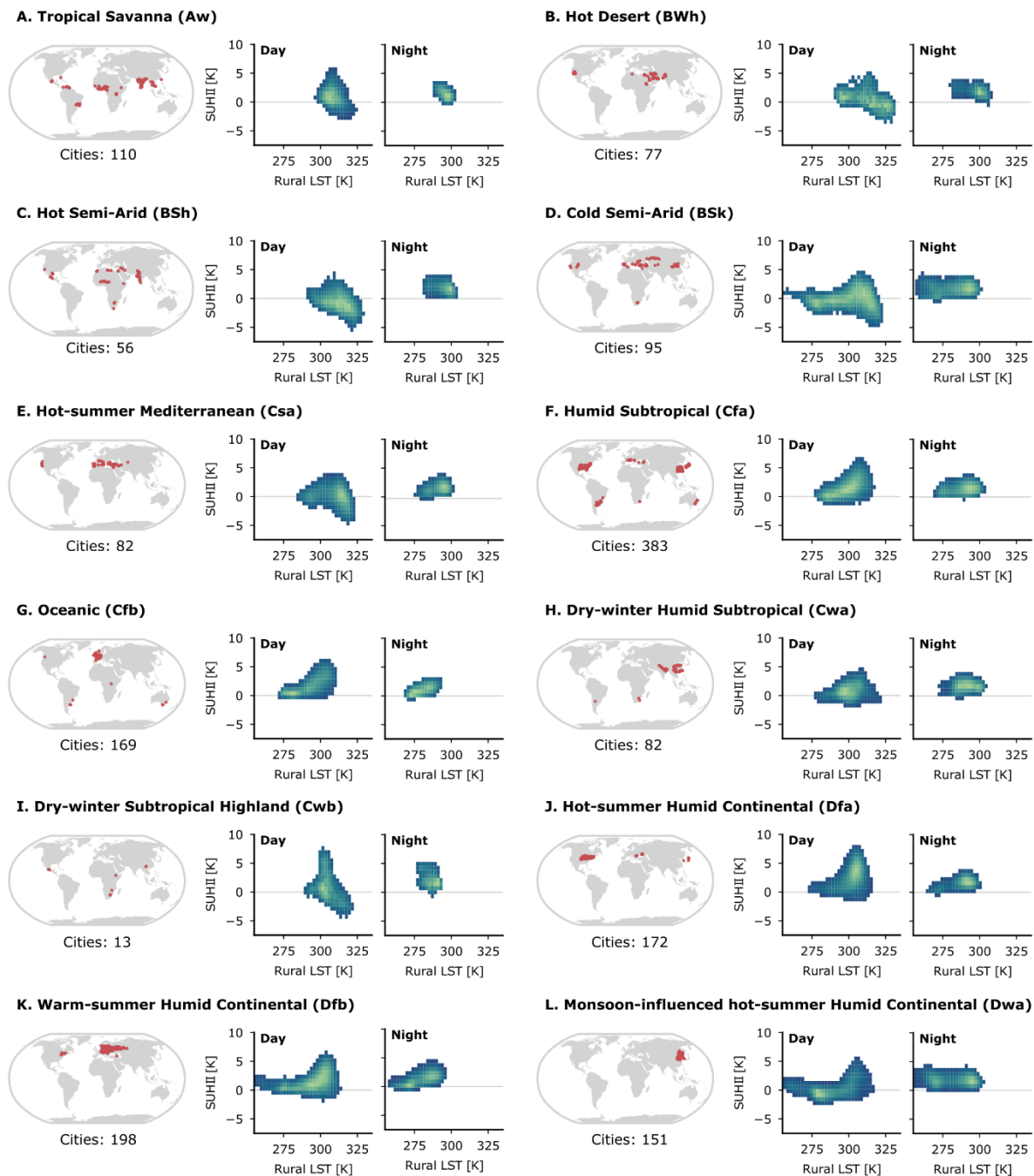
Figure 2-13: The daytime and nighttime SUHII climatology (2000-2018) in all the densely populated climates of Earth, visualized as the bivariate distribution of daily SUHII and rural LST.

Figure 2-15 presents the 1995-2018 daily 10:00/10:30 a.m. SUHII for Paris (France), Essen-Bochum-Dortmund (Germany) and Athens (Greece). Overall, the LST_cci 0.01° custom products provide consistent estimates of SUHII in terms of peak time. The SUHII magnitudes are also similar, but the estimates from the TERRA_MODIS_L3C 0.01° v1.0 data are somewhat warmer than those from the ERS-2_ATSR_L3C 0.01° v1.0 and ENVISAT_ATSR_L3C 0.01° v1.0 data products. This is especially apparent in Paris (Figure 2-15), where the maximum daytime SUHII for the years 2000 - 2018 is approximately 7 K for Terra MODIS and 5 K for ENVISAT and ERS-2. The difference between the MODIS and ENVISAT SUHII estimates is partially attributed to differences in the sensing time of the two instruments, which are not adjusted to a common overpass time in the LST_cci products. From Figure 2-15 it also clear that there are outliers present in the SUHII data derived from the TERRA_MODIS_L3C 0.01° v1.0, ERS-2_ATSR_L3C 0.01° v1.0 and ENVISAT_ATSR_L3C 0.01° v1.0 data products. These are mainly caused by calculating the daily spatial means from unequal data samples, which leads to biased estimates of $\overline{LST}_{urban}$ and $\overline{LST}_{rural}$, and are relatively few.
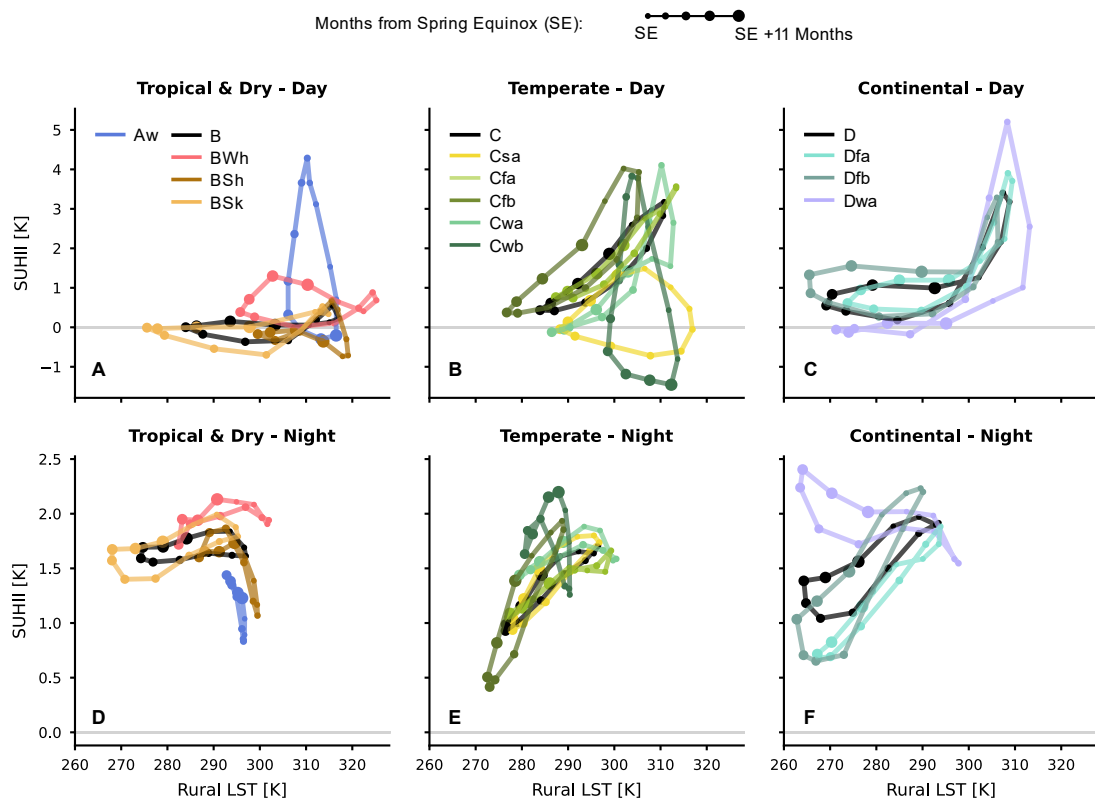
Figure 2-14: The daytime and night-time SUHII hysteretic curves for the 12 climate zones covered in this study derived from TERRA_MODIS_L3C 0.01° v1.0 LST_cci data product for the years 2000-2018. The curves corresponding to the dry, temperate, and continental parent-class curves are also presented in black.

The SUHII data presented in Figure 2-13, Figure 2-14 and Figure 2-15, agree with the published literature [RD-15, RD-16] and reveal the strong influence that local climate conditions exert on SUHII seasonality. In particular, in wet temperate and continental climates (e.g. Cfb, Dwa and Dfa) the daytime SUHII cycles are highly-similar and show a clear concave-up pattern. In dry climates (e.g. BSh, BSk, and Csa) the daytime SUHII cycles are more dissimilar and exhibit strong intra-class disparity. This is partially explained by the

greater susceptibility of dry-climate cycles to perturbations in the seasonality and magnitude of rainfall that makes their shape less stable than that of wet climates.

2.3.2.4 Conclusions

This study suggests that the 0.01° LST_cci TERRA_MODIS_L3C, ERS-2_ATSR_L3C and ENVISAT_ATSR_L3C custom products can be used for estimating SUHIIs and for describing their annual and seasonal variation. The SUHII characterisation in this study has primarily been achieved through the analysis of hysteretic curves. In general, the SUHII estimates calculated from the LST_cci MODIS, ENVISAT and ERS-2 products are consistent with each other, but some differences in the SUHII magnitudes may be observed. These differences are more pronounced between MODIS and ENVISAT SUHIIs than between ENVISAT and ERS. (It should be noted that the MODIS and ATSR instruments have differing algorithmic approaches, so some differences are expected.) The AQUA_MODIS_L3C 0.01° v1.0 custom data product was also trialled in this study, but it was found that the cloud contamination in this dataset was very severe and therefore it could not be used here. It is known that a new cloud detection approach has been developed for v2.0 of the LST_cci MODIS products.
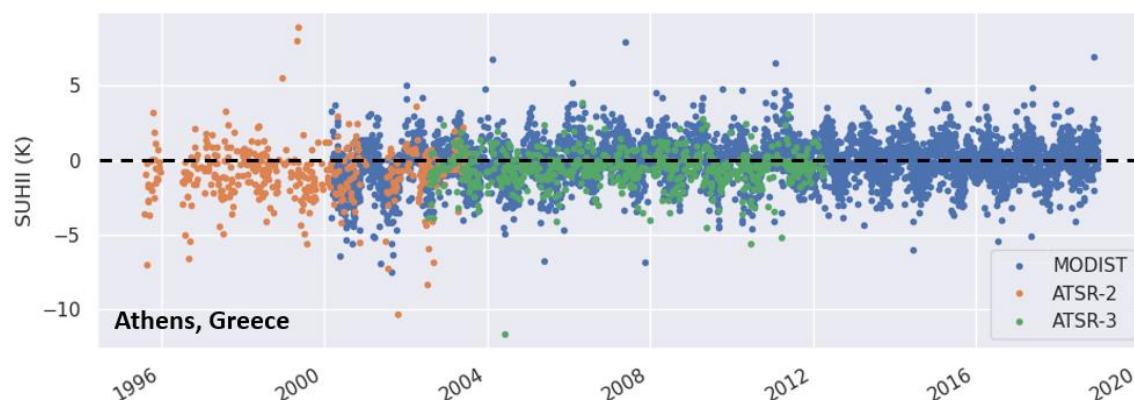
Figure 2-15: The daily SUHII for Paris, France, Essen-Bochum-Dortmund, Germany, and Athens, Greece, for the years 1995 to 2018.

2.3.3 Feedback on scientific utility of the LST_cci products

In general, the LST_cci 0.01° v1.0 custom products are easy to use and well documented. All the products used in this case study had the same variables and attributes, which facilitated their processing considerably. The main difficulty encountered in processing the LST_cci data was the mosaicking and stacking of the daily data over large areas, such as Europe, which is very memory demanding. Thus, it would be very useful if the data from each orbit were mosaicked beforehand and provided as tiles, similar to the gridded MOD11/MYD11 data products of NASA.

A major problem encountered during this study was cloud contamination, which necessitated pre-processing of the data to remove unrealistic outliers before the analysis was performed (see Section 2.3.2.2). This problem was particularly acute in the AQUA_MODIS_L3C 0.01° v1.0 custom data product, such that these data had to be excluded from the study. However, the problem with AQUA_MODIS_L3C was due to a bug in the v1.0 processing, which has been fixed for v2.0.

A further problem due to a bug in the v1.0 data used in this study was that LST data were originally retrieved for several sea grid cells close to the coastline, even under cloudy conditions. These grid cells had artificially low LST values and low values of uncertainties. This bug was also identified and fixed, and the data were reproduced for this study by the project team.

ATSR-data were also found to be missing over central India. However, this is a known issue with ATSR-2, as the data were never downloaded from the satellite in orbit through the mission in this region.

This case study relies heavily on ancillary LC data for identifying and delineating the cities in each LST image. Even though each 0.01° LST_cci netCDF file includes a variable with the LCC label of each pixel, it was found that this information did not change with time. Hence, in future releases, it is suggested the LCC data of each LST_cci netCDF file to change as a function of year.

In SUHI studies, SATZE (satellite zenith angle) is important for filtering and interpreting the LST. This is because the LST between east and west building facets can differ considerably within a day. Using the LST_cci data, this information cannot be obtained directly from the SATZE variable, but only after

combining it with the satellite azimuth angle (SATAZ). In future releases it is suggested that the SATZE angles are provided as signed floats where the "+" and "-" signs note if the satellite views the east or west side of the surface objects.

Finally, it was found that the latitude and longitude values of the global attributes "geospatial_lat_min", "geospatial_lat_max", "geospatial_lon_min", and "geospatial_lon_max" need to be corrected by half pixel in order to be equal to the actual bounding box coordinates of each LST image. The values currently provided are the latitudes and longitudes of the centre of the four corner pixels.

2.4 The role of LST characteristics in the data-driven simulation of terrestrial carbon fluxes (MPI-BGC)

2.4.1 Key Messages

❖ AQUA_MODIS_L3C 0.01° v2.0 and TERRA_MODIS_L3C 0.01° v2.0 are ingested into the data-driven modelling set-up 'Fluxcom2.0'. Their usefulness in the simulation of carbon and energy fluxes is tested in cross-validation experiments at eddy-covariance sites.

❖ Angular information and the change in v2 to provide instantaneous values, compared to averages potentially over multiple overpasses in v1.0, turned out very useful in this study.

❖ The availability of uncertainties is appreciated, but they were not useful for this application because large parts of the records were entirely removed by a threshold filter in uncertainties.

2.4.2 Scientific Analysis

2.4.2.1 Aims of the study

LST is one of the most influential factors on land-atmosphere fluxes of carbon, water, energy, and an important indicator of the state of the vegetation and land surface.

In this user case study, the role of LST in carbon and energy flux simulations is tested in the data-driven set-up 'Fluxcom' [RD-17]. Specifically, the contribution of MODIS LST to simulation accuracy of gross carbon uptake (GPP), sensible (H) and latent (LE) heat fluxes are analysed. The LST data used here are derived from IR observations and are therefore limited to clear skies; the influence of this bias in the availability for clear-sky-conditions only on the predicted fluxes is evaluated in this study. In addition, an analysis is performed to assess to what extent the acquisition properties of MODIS affect the simulations by simulating an LST from fixed viewing angles (as opposed to variable oblique views) and estimating LST at comparable observation times between overpasses (as opposed to variable observation time).

2.4.2.2 Data and Method

Land-atmosphere fluxes are estimated with the data-driven set-up called 'Fluxcom'. In this approach, machine learning models are trained with in-situ measured gross carbon, latent and sensible heat fluxes as target variables as well as with information on the state of the land surface (mostly space-borne) and with meteorological conditions as predictor variables. The trained model is then supplied with data sets of the same predictor variables used in the training to produce diagnostic estimates of the terrestrial

fluxes, but for a set of sites not seen in the training. In this study, the focus is on site-level evaluations rather than on spatially explicit estimates. In cross-validation experiments hourly land-atmosphere fluxes are estimated. Experiments with and without MODIS LST as predictors are performed at approximately 280 European flux tower sites, and the change in accuracy is assessed when LST is included as an additional predictor variable. As a measure of accuracy the Nash-Sutcliffe modelling efficiency (NSE) is used. Because LST is an integrator over a range of surface processes that work on a range of temporal scales, it is interesting to assess on which scales the accuracy changes most upon inclusion of LST as an additional predictor variable. The hourly flux estimates are aggregated to a mean diurnal cycle per month, to a daily mean seasonal cycle, to inter-annual changes. Also deviations from the mean seasonality and spatial between-site patterns are computed and the NSE change is analysed for each of the aggregated flux scales.

To assess the effect of variability in viewing geometry and overpass time, LST corrected to fixed viewing angles and observation times are ingested and their accuracy compared to experiments that use an LST with uncorrected viewing zenith angle and observation time. The effect of a clear-sky bias in MODIS LST is tested by training a model exclusively on clear sky days when all four MODIS LST are available. This ‚clear-sky model' is forced to generate estimates of the fluxes under all sky conditions. These clear-sky estimates are compared to the fluxes simulated by a model that was trained on data from both clear-sky and overcast days.

The MODIS data used in the study are shown in Table 2-5.

Table 2-5: A summary of the LST_cci products used in the study.

Product String and version	Sensor type	Resolution	Data availability	Local time of ascending node
TERRA_MODIS_L3C 0.01° v2.0	IR	0.01°	February 2000 – December 2018	22:30
AQUA_MODIS_L3C 0.01° v2.0	IR	0.01°	July 2002 – December 2018	13:30

For this, all MODIS LST_cci data streams are referenced to the locations of the eddy covariance (EC) sites for which good quality flux estimates are available. A single satellite pixel whose centre is closest to a tower location is selected in the current processing. This might entail a mismatch between the area of which the in-situ fluxes are representative and the size of the satellite pixel. In the current processing this is accepted and ways to account for spatial heterogeneity will be considered in future studies.

Quality checks on the MODIS LST_cci data using the provided uncertainty fields were unfeasible as too many data were removed when setting certain thresholds in uncertainty, while obvious residual cloud effects were not reliably detected. As a result, the ancillary data layers were not used, but an outlier detection algorithm was developed (Walther et al., 2021) [RD-40]. The approach is a modified version after Papale et al. (2006) [RD-18] and consists in checking distributions of consecutive LST values for unusually strong deviations (both positive and negative). As the dynamics of LST vary with the surface conditions, the distributions are grouped in temporal windows of several days.

Estimates of LST as if seen from a range of fixed viewing zenith angles (nadir, 10, 30, 50 degrees off nadir) are produced following Ermida et al. (2018) [RD-19]. It is worth noting that this analysis step was not possible with the LST_cci v1.0 data, which were originally utilised in this study. In light of this, customised v2.0 data were provided for this study, which use instantaneous rather than averaged LST values.

As the dynamics of LST in a day are strong, particularly during the MODIS/TERRA morning and MODIS/AQUA near-noon observations, the variable observation times of consecutive MODIS observations might introduce uncertainties and artifacts in the simulations of the fluxes. Therefore, an attempt is made to scale the MODIS observations to have them comparable in time (not for the near-noon overpasses). However, this scaling could introduce additional uncertainties that might be larger than in the uncorrected LST values. Thus, the effect of this observation time correction needs to be assessed. Again, this correction step would not have been possible with LST_cci MODIS v1.0 data, where data may be based on a number of overpass times.

MODIS LST_cci time series are gap-filled following a procedure described in Walther et al., (2021) [RD-40].

2.4.2.3 Results

Leaving out MODIS LST_cci as a predictor variable deteriorates model accuracy noticeably. The simulations of the energy fluxes appear overall slightly more sensitive to LST than GPP (Figure 2-16), and the contribution of LST to model accuracy is particularly pronounced on longer time scales such as the inter-annual (GPP, H) and deviations from the mean seasonality (all fluxes). Also between-site patterns of LE improve strongly from LST. The magnitude of the LST-related accuracy gain depends on how it is combined with other features, especially meteorological predictor variables. LST is particularly important if no meteorological variables are among the predictor variables (Figure 2-16). However, meteorological information is more important to the model than LST, as MODIS LST is not able to sufficiently inform the model on short-term variability in the hourly fluxes, and anomalies (deviations from the mean seasonality) are fully inaccurate without meteorology (not shown).

In dedicated evaluations along gradients in water availability and anomalies thereof (not shown) it is found that LST efficiently helps the models to more accurately represent effects of energy and water limitation on the fluxes and flux anomalies, again much more strongly in experiments without meteorological features than those in which meteorological information is present.

Results indicate that corrections for viewing zenith angles and observation time do not affect simulation accuracy. Independent of the flux considered and the feature combination, the magnitude of changes in model accuracy are in the range of the expected stochasticity of model accuracy (not shown).

Training a machine learning model only with ecosystem fluxes on clear days, when MODIS LST_cci observations are available, hardly affects the predictions and their errors for clear days. However, as shown in Figure 2-17 simulation errors on partly or fully overcast days (as defined by the ratio of actual and potential incoming short-wave radiation) increase strongly; relative absolute deviations reach 100% for GPP and LE. In terms of the predicted flux magnitudes, the clear-sky model produces about 50% higher GPP and LE estimates for overcast days than the all-sky model. H is extremely biased from the clear-sky model, up to 350% higher than estimates from the all-sky model.
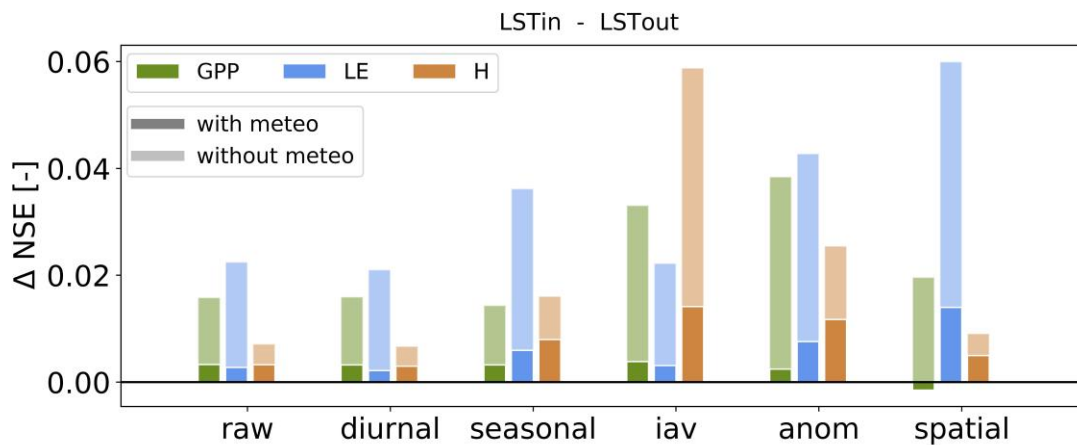
Figure 2-16: NSE gain when adding LST as predictors for experiments with and without meteorological features. The difference is computed as NSE of the experiment with LST minus the experiment without LST (LSTin - LSTout). GPP = Gross Primary Production, LE = Latent Heat Flux, H = Sensible Heat Flux. 'raw# refers to the actual hourly flux estimates, 'diurnal'= monthly mean diurnal cycle, 'seasonal'=daily mean annual cycle, 'iav'=inter-annual, 'anom'=deviations from the daily mean seasonal cycle, 'spatial'=patterns between site means.
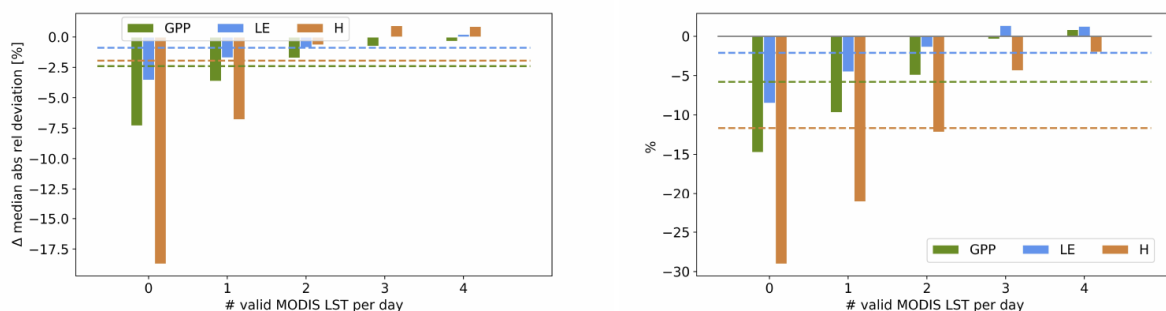
Figure 2-17: Effects of a clear-sky bias on prediction performance (left) and predicted values (right) along a gradient of cloudiness. Left: Accuracy gain in all-sky model relative to clear-sky. Each bar shows [MAD[all–sky training] - MAD[clear–sky training]]/ observation. Right: Percent under-prediction from experiments trained on all-sky conditions relative to predictions from clear-sky models. Each bar shows [sum(all-sky prediction[all-sky model]) - sum(all-sky prediction[clear-sky model])]/sum(all-sky prediction[clear-sky model]). Cloudiness index is defined as the ratio of short-wave incoming radiation/ potential short-wave incoming radiation. Potential short-wave incoming radiation has been linearly scaled to the 95th percentile per site before taking their ratio. Bins contain only days with at least 17 hours of good quality data in the eddy-covariance variables (all-sky) and during the growing season (EVI>30% of seasonal amplitude per site). Predictions per bin are consistently sampled across ecosystem fluxes. Dashed lines indicate the overall under-prediction by the all-sky model (unbinned).

2.4.2.4 Conclusions

MODIS LST_cci data turned out very valuable and useful for the data-driven simulation of land-atmosphere fluxes. Uncertainty information was not useful for filtering out low quality data in this application. However, in future experiments the uncertainties could be provided to the machine learning

model as another predictor variable to let the algorithms find the best way to handle the uncertainty information. Improvements in model accuracy brought by LST were overall strongest for deviations from the mean seasonality of the fluxes and inter-annual variations. Geostationary LST products, such as the SEVIRI LST_cci, might boost model performance through their high temporal resolution. The spatial scale-mismatches between the relatively larger geostationary footprint and the area that the in situ measured fluxes represent are larger than in the case of MODIS LST_cci 0.01°. Whether this negatively affects model performance and how this relates to potential benefits from resolving the diurnal cycle will be an interesting study case for future investigations, for which the long record in SEVIRI LST_cci v2.0 (longer than in v1.0) will be useful as will the other geostationary data sets from MTSAT and GOES.

2.4.3 Feedback on scientific utility of the LST_cci products
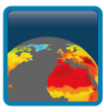
Working with the MODIS LST_cci 0.01° v2.0 data was straightforward and the meaning of the variables is clear. The availability of viewing and solar geometries in the files is highly appreciated.

This study was originally performed using v1.0 MODIS products, where grid cell LSTs may represent an average over multiple overpasses occuring at different times. For the v2.0 MODIS products, this approach was not used and the grid cell LSTs represent instantaneous LST values. This was found to be beneficial for processing steps such as geometrical corrections and a precise temporal allocation e.g. to ground data. However, it is recognised that instantaneous LST may be noisier with larger uncertainties. Discarded LST observations (that were previously used to produce the mean LSTs in v1.0) are not available to users in v2.0 data products. A recommendation from a user prespective is therefore to provide both instantaneous and averaged LST fields (despite the fact that also the number of ancillary fields on observation time and angles and uncertainties will be multiplied).

Independently of the product, gapfree LST data would be useful for several applications (including this one). However, requirements for strictness of quality control and therefore also gap structure will vary between applications, which might render this activity impossible.

The LST_cci MSG_SEVIRI_L3U v1.0 product was also trialled during the early phases of this study, which is available for the years 2008-2010. It was not used in the final study because in the limited time available no useful gap-filling method could be developed. Gapfree SEVIRI data would have been necessary to avoid clear-sky biases (as shown for the MODIS-related results above). Working with these data was mostly straightforward and the meaning of the variables is clear. The availability of viewing and solar geometries in the files is highly appreciated. Issues that have been noticed or aspects recommended from a user perspective are:

❖ Uncertainty information is only available starting from mid-2008 onwards, and the first period of available data in the record on uncertainty give negative values.

❖ The spatial extent of the SEVIRI disk changes at some point in the record, so only in the later part also northeastern Europe and parts of south America have valid data.

❖ The fields 'ncld' and 'variance' are included in the files but have no meaning as the values are instantaneous and nearest neighbor gridding was performed (personal communication with Sofia Ermida). As the LST_cci files have a standardized format across all products, a comment in the file attributes is suggested.

❖ Residual cloud contamination is detected.

❖ Requirements for LST characteristics vary between applications, therefore the following is suggested:

○ Provide the full SEVIRI record instead of limiting the available data to 2008-2010. Personal communication with Sofia Ermida revealed that a reprocessing with updated and extended data is planned soon. This reprocessing for the full record has happened in the meantime.

○ Include a geometrical correction factor for nadir view in the files (although it is acknowledged that the desirable reference angle might differ between applications).

○ High temporal and high spatial resolution at the same time is highly desirable. Downscaled geostationary LST would be of use for many applications.

○ Also depending on the application, instantaneous or temporally averaged LST might be preferable in terms of data availability, resolution and noise. Therefore, hourly averaged LST is suggested as an additional data layer.

2.5 Analysis of Urban Surface Temperatures in Romania (MeteoRomania)

2.5.1 Key Messages

❖ LST and T2m are compared in urban areas to explore the Urban Heat Island Intensity (UHII) at a country scale.

❖ The results show that LST and T2m are very well correlated in urban areas (r~0.9), particularly during the day.

❖ The surface UHII (SUHII), which is calculated from LST data, is influenced by local geography and varies spatially within the urban area.

❖ The MODIS/Aqua and MODIS/Terra LST_cci products are straightforward to use in urban climate research, but quality control related to cloud contamination is recommended.

2.5.2 Scientific Analysis

2.5.2.1 Aims of the study

The study aims at exploring the potential of the MODIS LST_cci products for performing (1) an inter-comparison between the LST and T2m in urban areas, and (2) exploring the Surface Urban Heat Island Intensity (SUHII) at country level, i.e. Romania.

2.5.2.2 Data and Method

The LST_cci products used in this study are customised TERRA_MODIS_L3C and AQUA_MODIS_L3C daily day/night 0.01° latitude/longitude v1.0 data over Romania (Table 2-6). The LST was extracted from both MODIS LST_cci data sets for 77 urban areas from Romania (> 30,000 inhabitants), for the period 2000-2018. In order to ensure a homogeneous data representation, only images with at least 50% data coverage for each city were selected. Extreme Outliers in the LST_cci data occur quite frequently, presumably due to cloud contamination, and these were removed and excluded from the analysis (see Section 2.5.3).

Table 2-6: A summary of the LST_cci products used in the study.

Product String and version	Sensor type	Resolution	Data availability	Local time of ascending node
TERRA_MODIS_L3C 0.01° v1.0	IR	0.01°	February 2000 – December 2018	22:30
AQUA_MODIS_L3C 0.01° v1.0	IR	0.01°	July 2002 – December 2018	13:30

The comparison between LST and T2m was performed for 6 cities of comparable size located in different geographic conditions, using the LST values of the pixel overlapping the WMO (World Meteorological Organisation) meteorological stations which monitor the local climate of each city. The LST_cci values with uncertainty greater than 2 K were not considered in the analysis.

The SUHII of each city with more than 30,000 inhabitants was computed both for daytime and night-time, as the difference between (1) the average LST of the urban pixels from the built-up administrative perimeter of each city, and (2) the average LST of the non-urban pixels from the surrounding rural buffer of each city. Water and wetland areas were excluded from the analysis.

The urban and rural areas were identified using the land cover information retrieved from CORINE Land Cover (https://land.copernicus.eu/pan-european/corine-land-cover).

2.5.2.3 Results

The results indicate very good correlations between LST and T2m for all the locations analysed both for daytime and night-time. For example, at the weather station at București-Afumați, -Băneasa, and –Filaret, which monitor the climate of Bucharest, the Pearson correlation coefficient is between 0.813 and 0.972 (Figure 2-18). The lowest correlations are found for summer, when the heterogeneity of the radiative budget may vary significantly over small areas due to influencing factors such as albedo, latent heat flux, or cloudiness.

Figure 2-19 and Figure 2-20 provide an overall view of the SUHII at country scale in July, which is generally the warmest month of the year in Romania. The SUHII data shown here are derived from an arithmetic mean of both MODIS/Terra and MODIS/Aqua data. For daytime, the lowest values can be observed in the southern areas due to either intense regional heating which as a result of two factors: (1) the regional extent and intensity of the warming dominates over the urban influence on the LST, and (2) the proximity of the Black Sea coast has a very strong influence on the urban climate in the SE areas. The highest SUHIIs occur in the North-Western part of the country, where the contrast between the built-up areas and regional background (i.e. very often the coldest area in Romania) enhances the SUHI formation and strengthening.

The T2m Urban Heat Island (UHI) is generally correlated with the size of the city [RD-20]. At country level, the SUHII is quite well correlated with urban surface area and population during the night-time (i.e. Pearson correlation coefficients 0.39, and respectively 0.38), while the daytime correlation is lower (Figure 2-21).
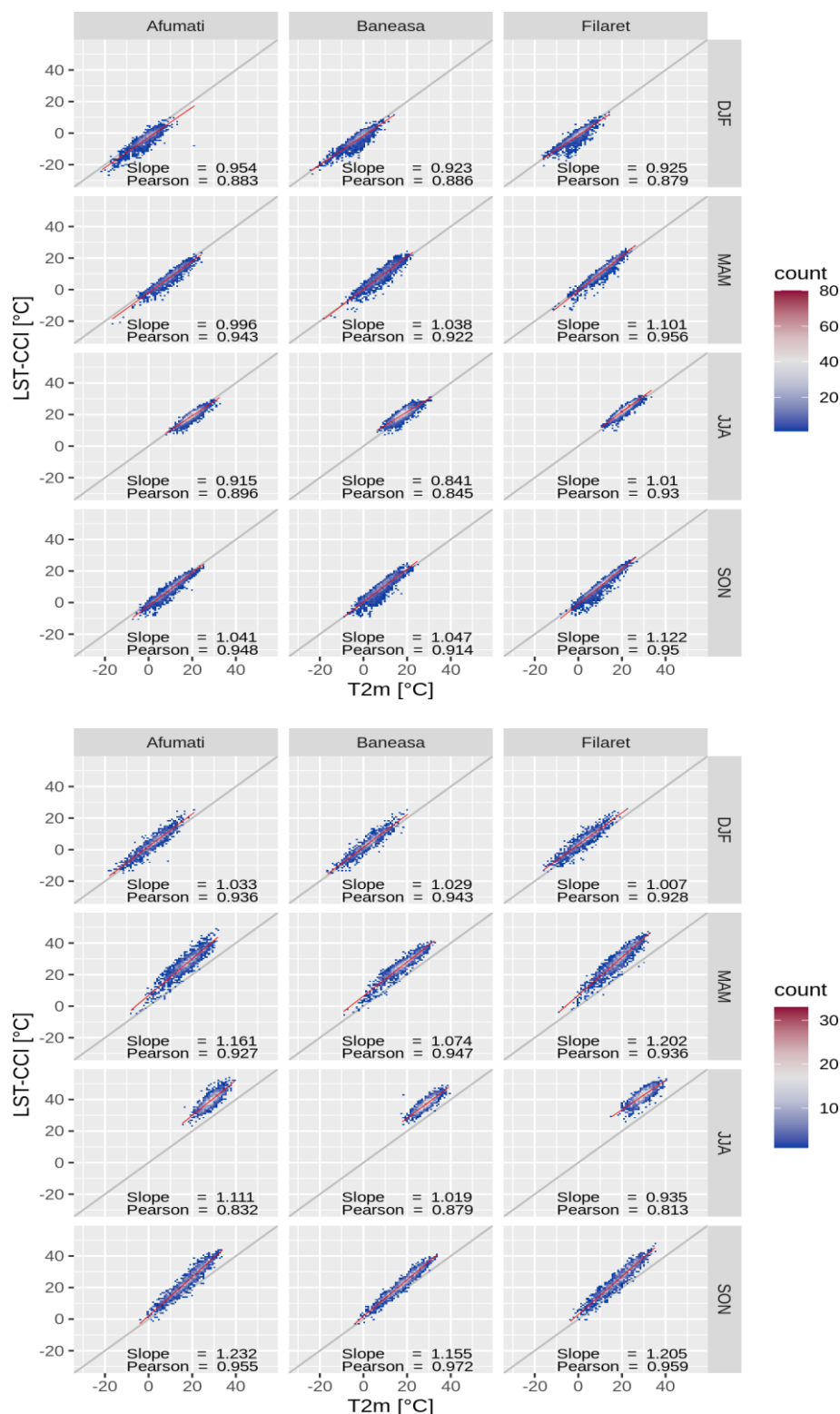
Figure 2-18: Comparison between MODIS LST_cci and T2m at the weather stations București-Afumați (peri-urban), -Băneasa (peri-urban), and -Filaret (urban), for night-time (upper) and day-time (lower)
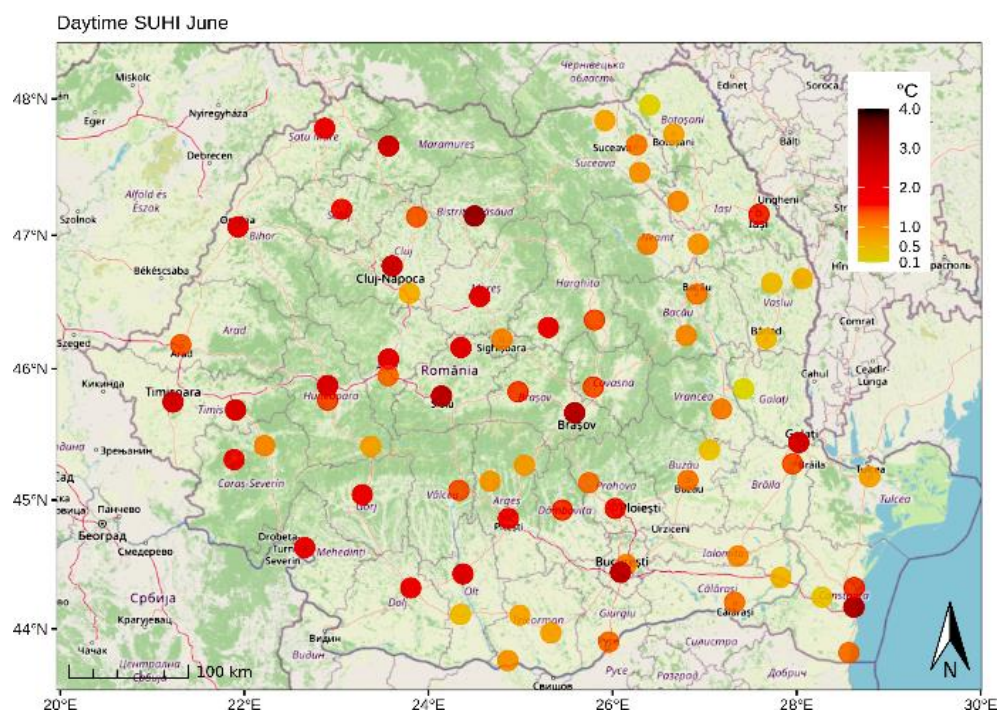
Figure 2-19: July daytime SUHII (°C) of the urban settlements with more than 30,000 inhabitants over Romania
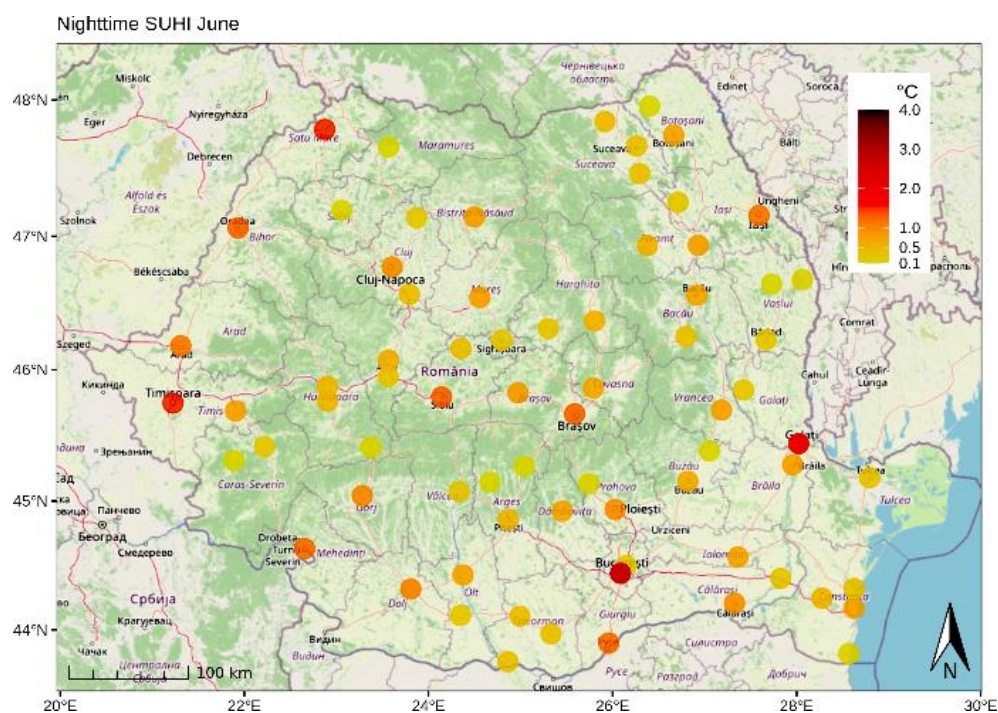
Figure 2-20: July night-time SUHII (°C) of the urban settlements with more than 30,000 inhabitants over Romania
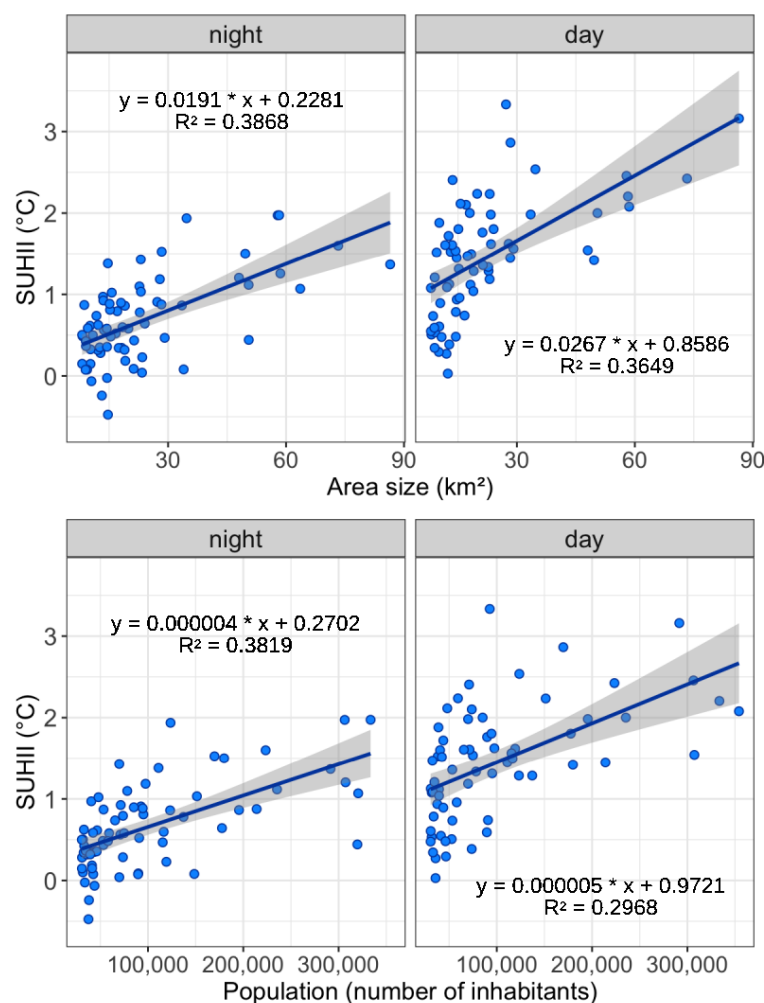
Figure 2-21: Scatterplot of average SUHII (°C) vs urban surface area and population in Romania

2.5.2.4 Conclusions

Based on analysis of the LST_cci MODIS 0.01° v1.0 products, this study demonstrates that LST and T2m are very well correlated over urban areas, especially considering the inherent differences related to the observations and temporal and spatial mis-match are considered (e.g. satellite areal average vs station point observation).

The data suggest that larger cities in Romania have considerable influence on the surface temperature, and the SUHI is clearly outlined both during day- and night-time. However, the regional geography has a strong impact on the SUHII, often dominating over the influence of the built-up areas in Romania, at least in the hottest months. The urban size (i.e. population and surface area) is more important for SUHII amplification during the night.

2.5.3   Feedback on scientific utility of the LST_cci products

The LST_cci products can be used easily in urban climate research, as they provide adequate resolution, hold an excellent accuracy over the area of interest, and address very well the temporal coverage required in climatology.

Some shortcomings include possible outliers identified in the data sets, very likely due to the cloud contamination of images. For example, Figure 2-22 shows low daytime LST values over Romania at the end of June, i.e. below 40°C, leading to a temperature range above 82°C. A summary of such anomalous ranges extracted from the entire LST_cci dataset used in this study is presented for each season in Figure 2-23.

In order to improve the reliability of the results, the data were filtered out using the Rosner method, performed with the rosnerTest() function from the EnvStats R package [RD-21]. Firstly, the LST range was computed for each image as the difference between the percentiles 98 and 2, in order to eliminate the most prominent artefacts. Secondly, the Rosner's generalized extreme Studentized deviate test detected the outliers within the resulted datasets [RD-22, RD-23], and anomalous LST values were identified within 112 images, which were not considered for the analysis.

The study emphasizes that quality control is highly recommended when using the MODIS LST_cci products in urban climate research, and improvements of the product in this respect would be very useful for end-users. Significant improvements on data quality and cloud clearing have been made by the LST_cci Science Team for v2.0 products.

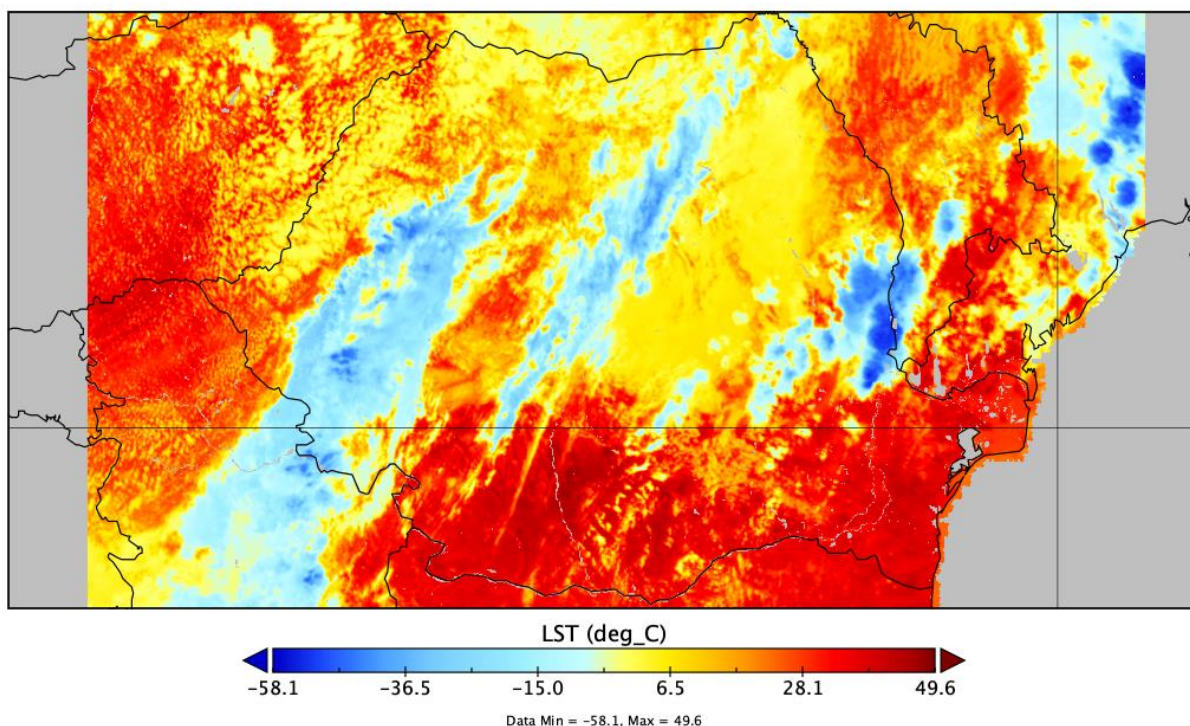ESACCI–LST–SE_–LST–MODIST–METROM–20000626095000

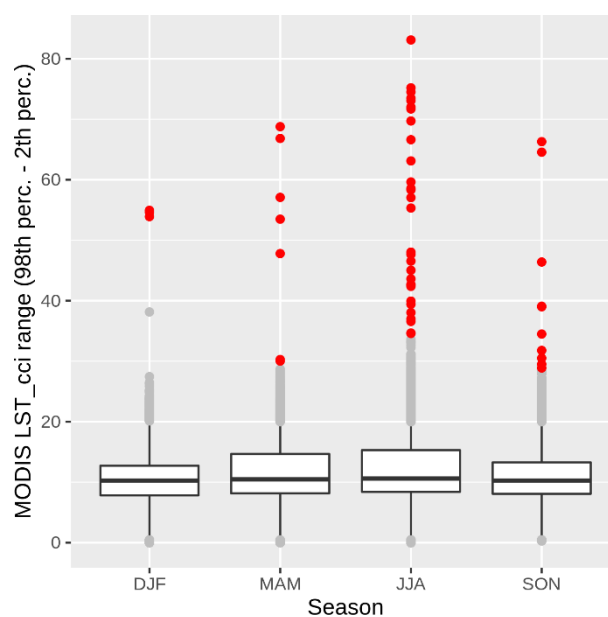*Figure 2-22: Land Surface Temperature over Romania on 26 June, 2000, 09:50 h UTC, extracted from MODIS/Terra*

Figure 2-23: Boxplots of the seasonal LST range values. Red dots are the outliers detected with the Rosner test, and not considered in the analysis

2.6 Integration of LST into a Surface Energy Balance Model (LIST)

2.6.1 Key Messages

❖ Daily LST day- and night-time pan-Australian mosaics are generated using AQUA_MODIS_L3C and Terra_MODIS_L3C 0.01° v1.0 LST_cci data products.

❖ LST data from several sites across the North Australian Tropical Transect (NATT) are integrated into a non-parametric Surface Energy Balance (SEB) model.

❖ The difference between LST and aerodynamic temperature (T0) is examined within the context of net available energy, fractional vegetation cover and soil moisture. It is found that LST and T0 can differ by several K, depending on meteorological and site conditions.

2.6.2 Scientific Analysis

2.6.2.1 Aims of the study
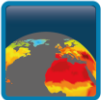
Radiometric surface temperature (LST) obtained from thermal infrared (TIR) remote sensing is routinely used as an approximation for aerodynamic temperature (T0) in evaporation and sensible heat flux mapping through surface energy balance (SEB) models. However, the relationship between the two temperatures is non-unique and not well known. While LST corresponds to a weighted soil and canopy temperature as a function of radiometer view angle, T0 represents the extrapolated air temperature profile at an 'effective depth' (called 'source-sink' height) within the vegetation canopy at which the sensible heat flux (H) arises. LST and T0 differ by several degrees, leading to large errors in evaporation (or latent heat flux, LE) estimates in arid and semiarid ecosystems. Despite several studies using one-source and multi-source SEB models attempting to accommodate the inequality of LST and T0, the 'kB-1-extra conductance' concept applied in one-source models questions their theoretical soundness. Contrasting empirical parameterizations of aerodynamic conductance to segregate the soil-canopy component temperature in the two-source models very often questions the appropriateness of such approaches. By using an analytical evaporation model, this study demonstrates direct retrieval of T0 and investigates aerodynamic versus radiometric surface temperature paradox for a broad spectrum of ecohydrological regimes in Australia. The study uses v1.0 LST data from the LST_cci project, which are integrated into a SEB model.

2.6.2.2 Data and Method

Table 2-7: LST_cci products used in this study

Product String	Sensor type	Resolution	Data availability	Local time
TERRA_MODIS_L3C 0.01° v1.0	IR	0.01°	Jan 2010 – Dec 2018	10:30 22:30
AQUA_MODIS_L3C 0.01° v1.0	IR	0.01°	Jan 2010 – Dec 2018	01:30 13:30

The LST_cci data used in this study are shown in Table 2-7. Mosaics were generated by sorting the datasets according to their filename by sensor, date and time stamp (day/night) separately. Accordingly,

the first tile of MODIS Aqua/Terra day- or night-time in the corresponding folder was defined as reference and all tiles within this folder updated this matrix by replacing NaN values with valid LST_cci data. This results in daily pan-Australian mosaic for MODIS Aqua or Terra day- or night-time, respectively. Afterwards subsets for the test sites were created. For each site, a block of 3 x 3 pixels surrounding each Eddy Covariance (EC) site was extracted and statistical analysis performed (e.g. mean, median, standard deviation); the mean LST is retained and is used to drive the SEB model.

The SEB model used here is called STIC (Surface Temperature Initiated Closure) [RD-24, RD-25, RD-26, RD-27], which integrates LST into the Penman-Monteith energy balance equation (PMEB) for simultaneous retrieval of T0, biophysical conductances, LE and H. T0 retrieval through STIC forced with LST from the LST_cci project, and in-situ meteorological datasets are evaluated against an inverted T0 retrieved from flux observations in water-limited (arid and semi-arid) and energy-limited (mesic) ecosystems from 2011 to 2018.

2.6.2.3 Results

Comparison of STIC T0 versus inverted T0 (Figure 2-24a - c) for the observed range of sensible heat flux (H) reveals significant correlation (r = 0.76 - 0.88, p-value<0.05) between them with a heteroscedastic pattern in the semiarid ecosystems. The differences between them consistently increase with increasing sensible heat flux (200 - 600 W m-2). The mean difference between the two temperatures is about -3.22 to 0.72°C, with Root Mean Squared Difference (RMSD) of 3.44 to 7.17°C and high systematic RMSD (57%) in the semiarid ecosystem. The difference between STIC and inverted T0 has a strong (moderate) and significant correlation with the product of wind speed and surface air temperature difference (udLST) in the arid (semiarid and mesic) ecosystem (r = 0.61, and r = 0.20 - 0.21, p-value<0.05) (inset of Figure 2-24a - c). This difference is likely to be related to assuming a constant parameter in the aerodynamic conductance estimation and its subsequent effects in T0 estimation, which could not meaningfully capture the expected variation in inverted T0. However, the range of errors associated with remote sensing derived LST could also be responsible for the differences between STIC T0 and inverted T0.

Independent comparison of STIC T0 with in-situ radiometric surface temperature (LST) for a wide range of fractional vegetation cover (fv) reveals STIC T0 to be consistently exceeding in situ LST in the arid (10 - 15°C) and mesic ecosystems (5 - 6°C) (Figure 2-24d, f) and their difference increases with increasing LST. A systematic relationship between the two variables (r = 0.95 - 0.98) is noted where T0 is a linear function of LST with slope and intercept of 0.90 - 1.11 and 2.38 - 5.53, respectively. A significant correlation between LST-T0 versus udLST (r = 0.12 - 0.49, p-value<0.05) was also noted and the direction of relationship changes in the mesic ecosystem (inset of Figure 2-24d - f).

In the arid ecosystem, there is clear evidence of a functional relationship between in situ LST-T0 and shortwave radiative heating (RG) (r = 0.54 [p-value<0.05], slope = -0.006, intercept = -0.866) for the entire range of soil water content (SWC) (Figure 2-24g). While the magnitude of the difference between LST and T0 increases with increasing RG, for a constant RG, T0-LST increases with declining SWC (Figure 2-24g). Similar behaviour is also evident in the mesic ecosystem, however, with less correlation strength (r = 0.23, p-value<0.05) and less steep slope (slope = -0.002, intercept = -2.692) (Figure 2-24i). No apparent pattern between in situ LST-T0 versus RG scatter was evident for the semiarid ecosystem (Figure 2-24h) and T0 exceeds LST mostly under low SWC and fv for the entire range of RG.

The scatterplot of β (= dT0/dLST) versus RG for the entire range of SWC (Figure 2-24j -l) and fv (inset of Figure 2-24j -l) further reveals that the temperature difference is the same only when high SWC and fv is associated with high RG. The contribution of LST on longwave radiation from the warm soil surface below the canopy results in such differences when both SWC and fractional vegetation cover is low and surface radiative heating is high.

2.6.2.4 Conclusions

Tiled LST_cci v1.0 data for MODIS Aqua and Terra at 0.01° latitude/longitude have been used to produce pan-Australian day- and night-time LST data sets for the period January 2010 – December 2018. Data corresponding to several EC sites in Australia have been extracted. Several of the sites suffer from frequent missing data, which is assumed to be due to cloud (expected for very humid sites with frequent cloud cover); unfortunately, these sites have too few data to be of use in this study so have been excluded from the analysis.

The LST_cci data have been integrated into a SEB model, which is used to estimate aerodynamic temperature, T0. The relationship between LST and T0 is explored for different site aridity, examining the effects of sensible heat flux, fractional vegetation cover, shortwave radiation, and soil water content. It is found that LST and T0 can differ by several K, depending on meteorological and site conditions.
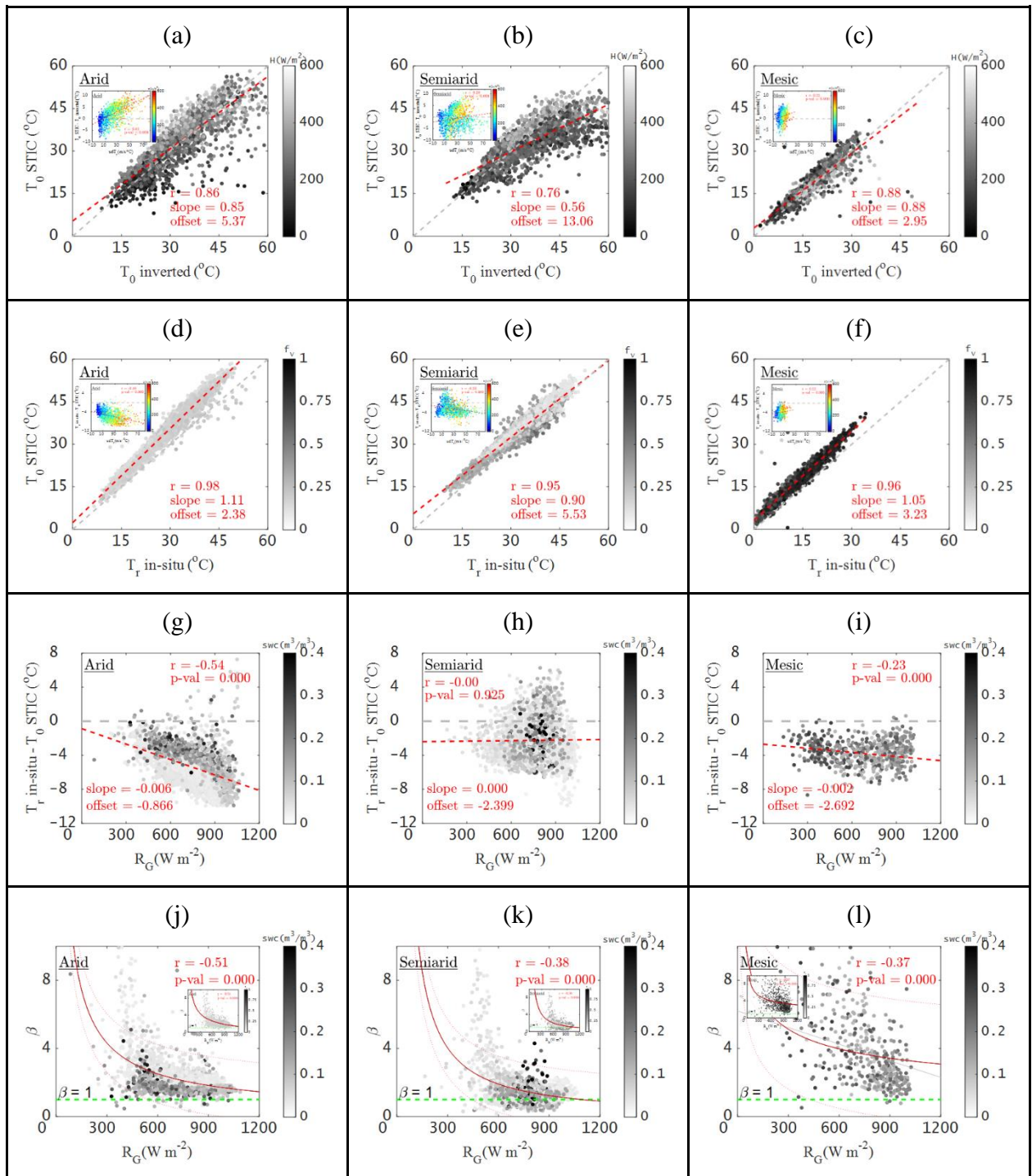
Figure 2-24: *(a)-(c) Comparison between retrieved T0 from STIC and inverted T0 by pooling data from all the arid, semiarid and mesic sites. The figures in the inset show how the differences between STIC T0 and inverted T0 depend on the product of wind speed (u) and LST-air temperature difference (dLST) with confounded effects of sensible heat flux (H). (d)-(f) Comparison between retrieved T0 from STIC and in-situ LST by pooling the data of all the arid, semiarid and mesic sites. The figures in the inset show how the differences between LST and T0 depend on the product of u and dLST with confounded effects of sensible heat flux (H). (g)-(i) Scatterplot showing the relationship between LST-T0 differences with shortwave radiation (RG) for the entire range of soil water content (SWC). (j)-(l) Scatterplot showing the shape of the relationship between β [(T0 – Ta)/(LST – Ta)] and RG for a wide range of soil water content (SWC) and fractional vegetation cover (fv) (in inset). Ta=air temp, Tr=LST.*

2.6.3 Feedback on scientific utility of the LST_cci products

Although the netCDF LST_cci products were well structured and easy to process in Matlab, naming the LST_cci tiles with a geo-location would be helpful or providing with a clear identification according to the MODIS tiling system or for example the Sentinel-2 tile grid (UTM system). This would make the identification of tiles containing the LST_cci data of the areas of interest easier. For example, the FLUXNET stations "Alice Springs Mulga" and "Ti Tree East" are both located in the Sentinel-2 tile 53KLR. With this identification code in the filename it would be easy to directly point to the areas of interest.

The availability of data due to cloud was found to be problematic and resulted in several sites not being useable in this study, as they did not have enough observations.

It is understood both these issues have been addressed by the LST_cci Science Team for the next releases.

3. Other User Case Study Reports

3.1 Demonstrate the potential of using a new metric: LST minus air temperature, to evaluate vegetation moisture stress in CMIP6 models (Debbie Hemming & Rob King, MOHC)

3.1.1 Key Messages

❖ Preliminary analyses have examined seasonal mean LST minus near-surface air temperature differences (LST-T2m) using data from UKESM1 (UK Earth System Model 1) and focusing on areas of grass and crop vegetation with either a C3 or C4 photosynthetic pathway. Two large regions, North America and China, have been examined.

❖ Differences in physiology between C3 and C4 vegetation means that C4 generally transpire less and show more tolerance to higher temperatures and lower soil moistures compared to C3. With lower transpiration rates, lower surface cooling is expected for C4 vegetation, and it is therefore proposed that areas dominated by C4 vegetation should show a larger mean LST-T2m and larger seasonal change relative to areas dominated by C3 vegetation.

❖ Results for North America and China show consistently larger differences and seasonal variations in LST-T2m for areas dominated by C4 (grass and crop) vegetation, compared with those dominated by similar C3 vegetation.

❖ Further initial work (not presented here) to study LST-T2m using LST_cci and ERA5 near-surface temperature has begun in preparation for the evaluation of CMIP6 models.

❖ A diagnostic for ESMValTool is presented. This compares the LST_cci to CMIP6 models. An example using UKESM is shown, where the uncertainty information presented comes from the model data. A second diagnostic is under development that exploits the uncertainty information given in the LST_cci product.

❖ Initial work to implement the diagnostic for ESMValTool highlighted a minor issue with the coordinate metadata in the AQUA_MODIS_L3C V1.0 product which showed two latitude coordinates (rather than latitude and longitude) in the 'standard name'. This has now been corrected for further updates of the data (see section 2.1.3).

3.1.2 Scientific Analysis

3.1.2.1 Aims of the study

Land Surface Temperature (LST) provides information on the partitioning and exchanges of energy and water between the land surface and atmosphere. It also influences the timing and productivity of terrestrial vegetation through availability of energy for photosynthesis and evapotranspiration, which exerts a key limitation on vegetation moisture availability. This study aims to assess the potential for a new vegetation stress metric, namely LST minus air temperature (LST-T2m) that can be used for evaluation of large-scale vegetation moisture stress in Earth System Models (ESMs).

Initial analyses for the CMUG and presented here utilise as a first step LST and near surface air temperature from UKESM1 to analyse spatial and temporal variations in LST-T2m for two major biomes (C3 and C4 grass and crop types) across two large regions, North America and China. Physiological

differences between C3 and C4 vegetation at the leaf level are expected to show as larger LST-T2m differences across large-scale C4 dominated areas [RD-28].

The results presented here use the land cover from UKESM1 but this work will progress to use biomes characterised using LC_cci Land Cover data, and further work will utilise Soil Moisture data from SM_cci to understand relationships between LST-T2m and moisture stress. The work will address two key science questions: i) Can the LST-T2m metric be used to monitor global-scale vegetation moisture stress across different biomes and regions? and ii) How well do CMIP6 ESMs capture spatio-temporal trends in LST-T2m?

Further to this, a diagnostic using the LST_cci product has been developed as part of the CMUG project. This compares the LST over a specified region to the corresponding area in one or more CMIP6 models. An ensemble mean can be compared by using multiple ensembles from the same CMIP6 model or even from multiple models. Although LST_cci has a variety of sensor platforms to work with, this work has concentrated on using the AQUA_MODIS data. This is so the diagnostic can support vegetation-based research with Aqua's local overpass time being early afternoon, similar to the peak vegetation activity.

3.1.2.2 Method

LST-T2m differences were examined using output from historical runs of UKESM1 exploiting the monthly mean output stream. For the two areas of interest, North America and China, the ensemble average plant functional type was used to create a seasonal land cover mask for the years 2003-2014. Grid boxes were classified as either C3 or C4 grasses and crops if they covered at least 50% of the grid box area. Seasonal mean LST-T2m values were produced for each of the C3 or C4 masked regions.

In order to compare monthly LST data with the CMIP6 models, a monthly LST value that represented the whole day is needed. To do this, a CMORizer script has been written as part of ESMValTool that creates an 'all time' monthly LST value by taking the mean of the daytime and night-time overpass values given by LST_cci from the monthly version of the product not the daily version.

3.1.2.3 Results

Preliminary results show clear differences in the LST-T2m differences of C3 and C4 vegetation (Figure 3-1; note the results presented are for modelled data not the LST_cci products). For two large-scale regions, China and North America, areas dominated by C4 vegetation show consistently larger seasonal mean LST-T2m differences compared to C3 dominated areas. The seasonal cycle of LST-T2m for C4 vegetation is also up to 3 times larger across China and about two times larger across North America than for C3 vegetation.

These initial results are consistent with expectations based on physiological differences between C3 and C4 vegetation that lead to generally warmer leaf surface temperature of C4 vegetation, due to lower transpiration rates, compared with C3 vegetation. This difference is accentuated during warmer, drier periods as shown by the larger difference between C3 and C4 dominated areas during summer in both regions.

The results indicate that the LST-T2m metric is able to identify large scale spatio-temporal variations in moisture status of dominant vegetation.

An example of the diagnostic output is given in Figure 3-2. This shows the LST difference, given as LST_cci minus ensemble mean of UKESM, over a region of North America shown in Figure 3-3. This shows the standard deviation of the differences giving a measure of the spread of LST. In this case, the smaller the spreads, the better the model ensembles match the LST_cci product.

3.1.2.4 Conclusions

Physiological differences between C3 and C4 vegetation result in consistently higher leaf temperatures for C4 vegetation. Preliminary results show that these differences are clearly evident in the seasonal LST-T2m difference across two large regions, China and North America.

Further work for this study will assess the potential for the LST-T2m difference to be used as a large-scale evaluation metric for vegetation moisture stress responses in ESMs by using the LST_cci as an observation truth to evaluate against.

This work is continuing to develop a diagnostic for ESMValTool that exploits the uncertainty information given by the product. The aim is to present both a measure of the model ensemble spread and the total uncertainty in the LST_cci product over the test region.

3.1.3 Feedback on scientific utility of the LST_cci products

Initial work with monthly mean AQUA_MODIS_L3C V1.0 LST_cci products has shown that the data are easy to download and manipulate for inclusion in ESMValTool. This will allow the work to evaluate UKESM1 and other CMIP6 models using the above described methods with the LST_cci product. A minor issue with the header information of the AQUA product was noted, where the 'standard_name' included two latitude coordinates, rather than latitude and longitude. This was important to correct for converting the MODIS_L3C products to a format suitable for inclusion into ESMValTool. After discussions between the LST_cci science team and CRG, the standard name was corrected for the next update (v2.0) of the relevant LST_cci products.
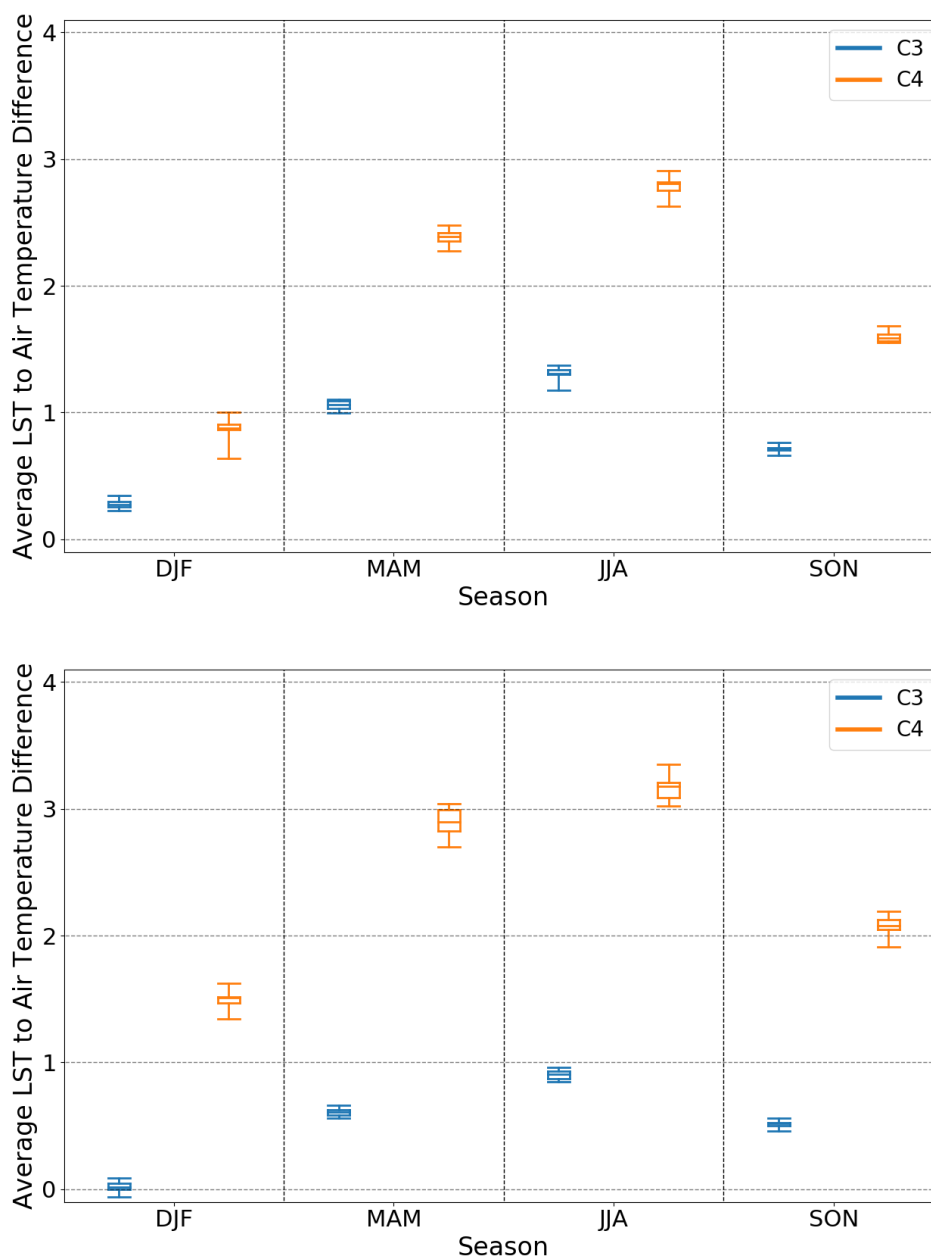
Figure 3-1 Seasonal mean variations in model LST-T2m (°C) for areas dominated by C3 (blue) and C4 (orange) grass or crops across China (upper) and North America (lower). Boxes show the 25th and 75th percentiles, with the line in the box representing the median value. The whiskers show the minimum and maximum values of the variation across all years 2003-2014 inclusive (within the region).
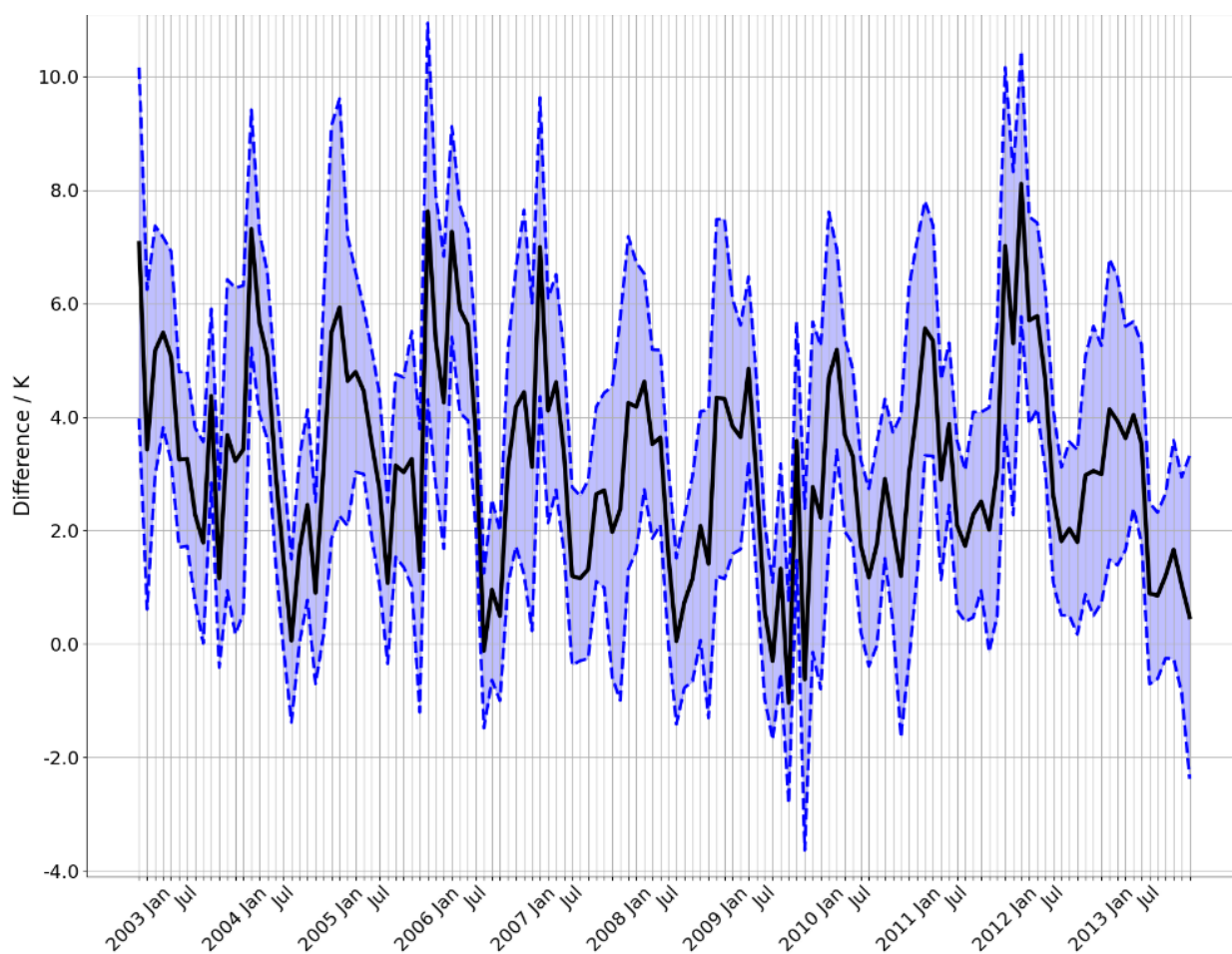
Figure 3-2: The difference between LST_cci and the ensemble mean LST from UKESM (solid black line). The blue shaded region denotes plus/minus one standard deviation from the mean difference using the spread of values from UKESM. This has been calculated from the area averages in the region of North America given in Figure 3-3.

LST / Kelvin
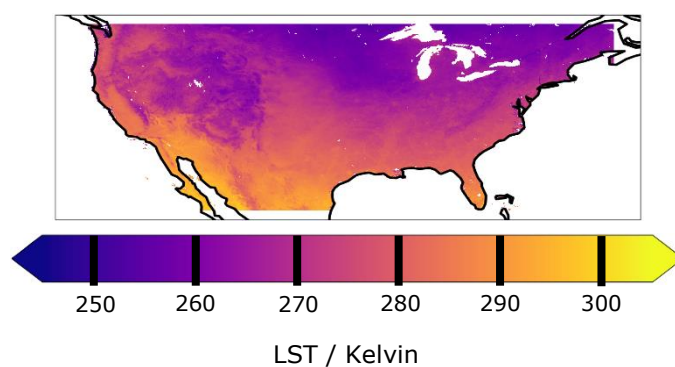
Figure 3-3: The 'all time' average (as described in the main text) of the AQUA_MODIS LST_cci for one month to show the region of North America Figure 3-2 is calculated over.

3.2 Evaluation of LST_cci MODIS products against ground data at the Valencia Test Site (R. Niclòs, University of Valencia)

3.2.1 Key Messages

❖ TERRA_MODIS_L3C / AQUA_MODIS_L3C 0.05˚ LST_cci products V1.0 and V2.0 were evaluated against ground data at the Valencia Test Site to test accuracies for meteorological and climate studies within the University of Valencia's research projects.

❖ Evaluations for the MODIS operational LST products (MOD/MYD11_L2 and MOD/MYD21) were also developed using the same ground data as reference data.

❖ The TERRA_MODIS_L3C / AQUA_MODIS_L3C version 2 products systematically overestimate (around 2 K) ground LSTs, also leading to root-mean-square differences (RMSD) of around 2 K (2.5 K for the TERRA_MODIS_L3C product). However, the overestimates have decreased as compared to those for version 1 products (of around 4 K).

❖ These overestimates of 2 K were not observed for the MODIS operational products.

❖ However it should be noted that the LST_cci input data used is at a different resolution (0.05˚) to the operational MODIS products (1 km) so the comparison to point scale in situ is not expected to yield comparable results. This is in contrast to the comparison in the PVIR [AD-02] which validates all the LST_cci products at their native resolution (so 1 km for MODIS).
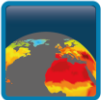
❖ The validation results at the Valencia Test Site are outliers compared to the results at the sites used in LST_cci and documented in the PVIR [AD-02].

❖ Although further evaluations should be done by analysing the results for version 2 LST_cci MODIS L2P products when available at our site, these preliminary results show that the systematic uncertainty has been reduced in version 2 L3C products, and thus it seems that the LST_cci project works on the right path to offer an accurate tool for analysing thermal trends in climate studies.

3.2.2 Scientific Analysis

3.2.2.1 Aims of the study

Versions 1 and 2 of the TERRA_MODIS_L3C / AQUA_MODIS_L3C products (i.e., MODIS LST_cci 5 km products both for EOS-Terra and EOS-Aqua overpasses, respectively) were evaluated against ground data at the Valencia Test Site [RD-29, RD-30] to test the accuracies of these Land Surface Temperature (LST) products for meteorological and climate studies within the research projects lead by the University of Valencia (e.g., project PID2020-118797RB-I00 funded by MCIN/AEI/10.13039/501100011033). The Valencia Test Site is a uniform and thermally-homogeneous rice paddy area, with very different land cover through the year due to crop phenology. Land cover includes water surfaces (in case of flooded soils), full vegetation cover and bare soils.

The MODIS operational products (MOD/MYD11_L2 and MOD/MYD21) versions v006 and v061, were also evaluated using the same ground data as reference data for comparison. These products are obtained with the generalized split-window (SW) algorithm [RD-31, RD-32] and the temperature-emissivity separation (TES) algorithm [RD-33, RD-34] respectively, and are disseminated through the NASA's Earth Data Search website (search.earthdata.nasa.gov).

The objective was also to contribute feedback to the LST_cci project, to generate more accurate LST products for climate applications.

3.2.2.2   Method

Ground TIR measurements were performed using several hand-held Cimel Electronique CE-312 radiometers. Measurements were acquired along predetermined transects over the test site and concurrently with MODIS overpasses in cloud-free conditions. The number of radiometers used ranged from 2 to 4 depending on the day. Radiometers were calibrated in the laboratory (each year) and within international campaigns, so the calibration uncertainty was estimated [RD-35, RD-36].

The ground measurements were acquired following the methodology described in [RD-29] for cloud-free days from 2016 to 2018 (daytime only). The CE-312 radiometers measured the surface radiance within a spectral band i, $L_{surf,i}$, which depends on the surface emissivity, ε_i, as follows:

$$\textbf{Equation 3-1} \quad L_{surf,i} = \varepsilon_i B_i(T) + (1 - \varepsilon_i) L_i^{\downarrow}{}_{a,hem}$$

where $B_i(T)$ is the channel Planck's function for a temperature T (here T being the LST). $L_i^{\downarrow}{}_{a,hem}$ is the atmospheric downwelling irradiance divided by π [RD-30]. $L_i^{\downarrow}{}_{a,hem}$ was measured using an Infragold Reflectance Target (IRT-94-100) made by Labsphere [RD-37], which is a highly diffuse gold panel with a reflectivity close to 0.92 in the 8 – 14 μm region.

Additionally, emissivities for the different land covers were measured at the site, and not assumed or estimated from threshold methods or databases. Emissivity measurements were taken using the TES method [RD-33, RD-38] applied to the ground data measured by the CE-312 radiometers and also the Box Method [RD-30].

The reference ground LSTs were obtained as the average of the LST measurements performed by all ground radiometers within five minutes of each overpass time.

3.2.2.3   Results

This section shows the results of the evaluations of the above mentioned LST_cci and operational LST products using the described ground data as reference (Section 3.2.2.2). Table 3-1 to Table 3-4 show the statistical differences of the product LSTs minus ground LSTs in terms of bias, standard deviation (SD) and root-mean-square differences (RMSD). Table 3-1 shows the results for version 2 AQUA_MODIS_L3C together with those for v006 MYD11_L2 and MYD21 products. Table 3-2 shows the same results for version 2 AQUA_MODIS_L3C but together with those when using the available v061 MYD11_L2 and MYD21 products for the study period. Table 3-3 shows the results for version 2 TERRA_MODIS_L3C together with those for v006 MOD11_L2 and MOD21 products. The same results are shown in Table 3-4 but in comparison with the available v061 MOD11_L2 and MOD21 products for the study period. Results are also shown in Figure 3-2 and Figure 3-3, including in this case version 1 LST_cci L3C results for comparison. Average LSTs weighted by the inverse of the squared distance to the site coordinates were obtained for the 2 × 2 closest pixels to evaluate the operational products.
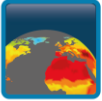
Table 3-1: Results of the evaluation of the day-time version 2 LST_AQUA_MODIS_L3C and the operational v006 products for EOS Aqua - MODIS.

	LST_AQUA_MODIS_L3C _v2 – LST_ground (K)	LST_AQUA_MYD11 – LST_ground (K)	LST_AQUA_MYD21 – LST_ground (K)
BIAS	1.9	-0.1	0.9
SD	1.1	0.8	1.1
RMSD	2.2	0.8	1.5
N. EVENTS	22	19	19

Table 3-2: Results of the evaluation of the day-time version 2 LST_AQUA_MODIS_L3C and the available operational v061 products for EOS Aqua – MODIS for the study period (only 7 matchups).

	LST_AQUA_MODIS_L3C _v2 – LST_ground (K)	LST_AQUA_MYD11 – LST_ground (K)	LST_AQUA_MYD21 – LST_ground (K)
BIAS	1.9	-0.2	0.8
SD	1.1	0.8	0.9
RMSD	2.2	0.8	1.2
N. EVENTS	22	7	7

Table 3-3: Results of the evaluation of the day-time version 2 LST_TERRA_MODIS_L3C and the available operational v006 products for EOS Terra - MODIS. No v006 MOD21 product was available for the study period.

	LST_TERRA_MODIS_L3C _v2 – LST_ground (K)	LST_TERRA_MOD11 – LST_ground (K)
BIAS	2.1	-0.2
SD	1.5	1.6
RMSD	2.5	1.6
N. EVENTS	31	28

Table 3-4: Results of the evaluation of the day-time version 2 LST_TERRA_MODIS_L3C and the available operational v061 products for EOS Terra – MODIS for the study period (only 8 matchups).

	LST_TERRA_MODIS_L3C _v2 – LST_ground (K)	LST_TERRA_MOD11 – LST_ground (K)	LST_TERRA_MOD21 – LST_ground (K)
BIAS	2.1	-0.9	0.0
SD	1.5	0.5	0.6
RMSD	2.5	1.0	0.6
N. EVENTS	31	8	8

Figure 3-4: Comparison of LSTs obtained for the site coordinates from the EOS Aqua – MODIS products against ground LSTs. Results for version 1 and version 2 AQUA_MODIS_L3C products and v006 MYD11_L2 and v006 MYD21 operational products are shown for daytime only, when ground measurements along transects were acquired.
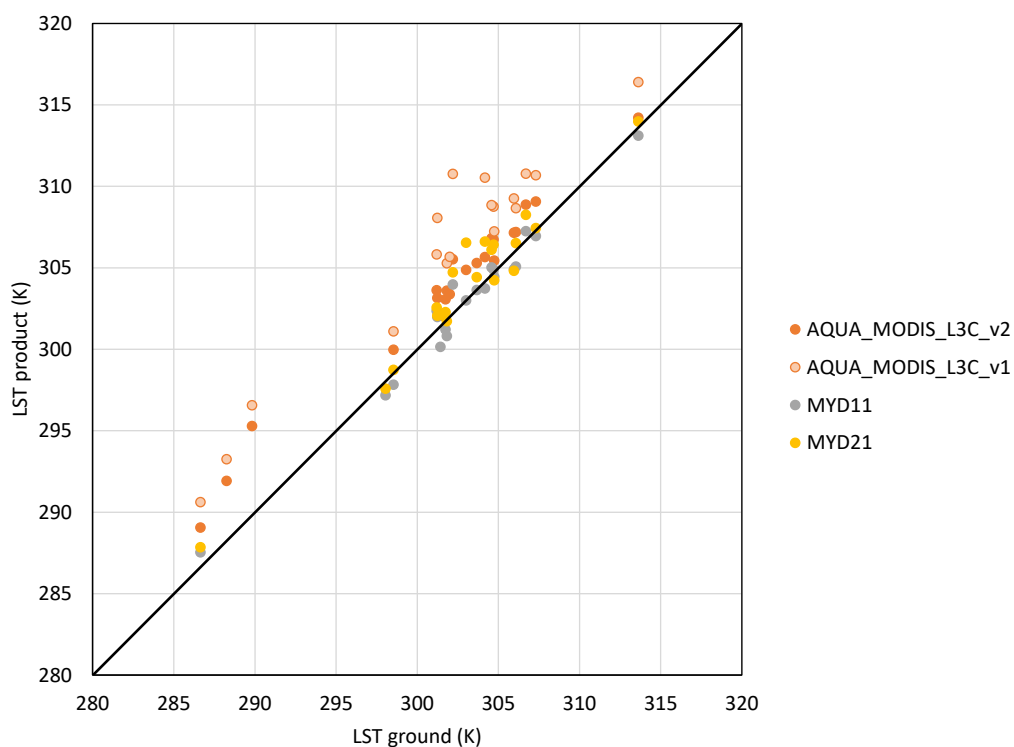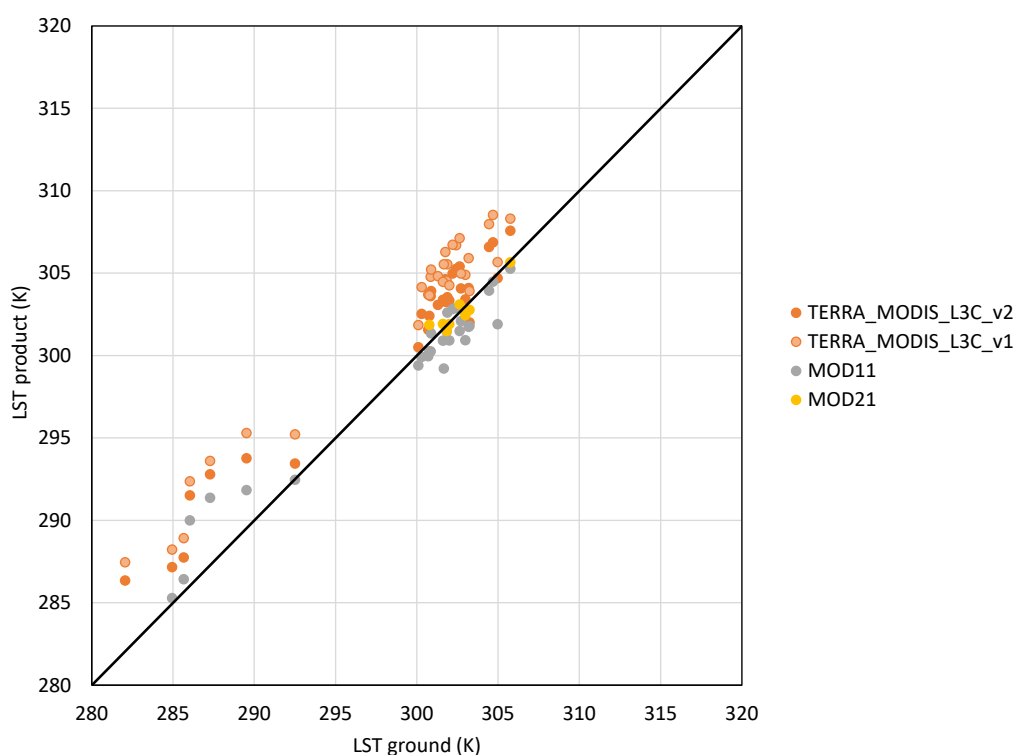
Figure 3-5: Comparison of LSTs obtained for the site coordinates from the EOS Terra – MODIS products against ground LSTs. Results for version 1 and version 2 TERRA_MODIS_L3C products and v006 MOD11_L2 and v061 MOD21 operational products are shown for daytime only, when ground measurements along transects were acquired.

Biases of 2 K and SDs up to 1.5 K are shown for version 2 LST_cci MODIS L3C products, leading to RMSDs of 2.2 K for AQUA_MODIS_L3C and 2.5 K for TERRA_MODIS_L3C (unlike the biases and RMSDs of around 4 K shown for version 1 LST_cci MODIS products in the previous report, and here in Figure 3-4 and Figure 3-5). Lower biases are shown for the operational products (e.g., negligible biases were obtained in the case of v006 MYD11_L2 and MOD11_L2 products), with similar SDs, leading to RMSDs lower than 1.6 K in all cases (and even lower than 1 K in the case of MYD11_L2).
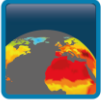
3.2.2.4   Conclusions

The results show that the version 2 of LST_cci MODIS L3C 0.05˚ products still overestimate ground LSTs (with bias and RMSD of around 2 K) both for EOS Aqua - MODIS and EOS Terra – MODIS. However, the overestimates have decreased as compared to those for version 1 products (of around 4 K). In any case, further evaluations should be done by analysing the results for the version 2 LST_cci MODIS L2P products at 1 km, when they are provided at our site. The 2 K systematic uncertainties are not observed for the operational products, neither in the case of the SW product (MYD/MOD11) nor in the case of the TES product (MYD/MOD21). The systematic uncertainties shown for the LST_cci products may be due to differences between the emissivities assigned for the site in the LST_cci products and ground-measured emissivities, which sharply varied in the evaluation dataset because of land cover type changes at the site across the year. However, the LST_cci emissivities are not provided in version 2 products (unlike in version 1 products), which would be advisable to evaluate possible differences with respect to the emissivities measured at the site for the different land covers.

3.2.3   Feedback on scientific utility of the LST_cci products

A few sentences summarising the experience with the LST_cci products in this study:

❖ products were accessible and easy to use since they were provided in NetCDF format, which is easily readable by several image processing software packages and programming languages.

❖ low spatial resolution for evaluation purposes in the case of L3C products if the region of interest is not homogeneous. The Valencia test site is quite homogeneous for the different land cover types across the year, as previously shown in the above mentioned references.

❖ no emissivity values were provided in version 2 LST_cci MODIS L3C products (unlike in version 1 products). However, emissivity is a key variable to obtain LST data.

❖ LST_cci products for other satellite sensors (e.g., MetOp-A/B/C AVHRR/3 and S-NPP/JPSS1 VIIRS) could be also interesting, as well as more availability of information about the algorithms, specific techniques, version 2 changes, and input data used to generate the LST_cci products.

3.3   Reports from other users

A further seven other known users have requested access to LST_cci data. All these users were contacted and asked for feedback (in any format) on their experiences so far. Only one user has responded to say that they had downloaded a few data files but had not progressed further than this with any analysis. This user reported they had no issues with getting hold of the data and loading into Python, etc.   As a non-expert in the use of satellite data, their main comment is that they found the directory structure quite confusing, with a lot of unexplained acronyms and recommended that a readme file for this beta data portal would be useful to help get them started.

4. Summary

This section synthesises the findings from the studies presented in Section 2 and Section 3 regarding the suitability of the v1 and v2 LST_cci products for climate applications. The following sub-sections summarise the conclusions from the overall climate assessment by theme. In response to feedback from users incorporated in the first Climate Assessment Report, LST_cci v2 products have been improved substantially. Although, these improvements have not been fully assessed in this second CAR due to the timing of data availability, some initial assessments have been made that will inform future developments.

4.1   Data set accuracy, stability and precision

The accuracy, precision and stability of the LST_cci data sets is being assessed through a dedicated validation work stream within the LST_cci project and is reported elsewhere. However, three of the UCS and one other user study have compared the LST_cci data sets with other surface temperature observations that provide insight into the performance of these data: 1) LST anomalies from 0.05° L3 MODIS, ATSR-2, AATSR, SLSTR, and the MW and IR CDRs have been compared with collocated station T2m anomalies over Europe within the Met Office UCS, 2) MODIS L3 LST data (locally derived from MODIS L2 1km data) have been compared with airborne LST observations over Greenland in the DMI UCS, 3) collocated 0.01° L3 LSTs and station T2m observations have been compared at urban locations in Romania within the MeteoRomania UCS, and 4) MODIS L2 and L3 LST data have been compared with in situ LST observations over a site in Spain. The following conclusions are based on these studies:

❖ A strong relationship between LSTs from LST_cci L3C v2.0 IR, SSMI_SSMIS_L3C v2.23 and MULTISENSOR_IRCDR_L3S v1.0 and collocated station 2m air temperature (T2m) observations is observed:

  ○ Anomalies for Tmean, Tmax and Tmin show reasonable correlations and slopes (r and m ≈ 0.6-0.9), with Tmin comparing less well than Tmean and Tmax.

  ○ Only the AQUA_MODIS_L3C and the ENVISAT_ATSR__L3C products appear stable; the TERRA_MODIS_L3C, ERS-2_ATSR__L3C, MULTISENSOR_IRCDR_L3S and SSMI_SSMIS_L3C products show non-climatic discontinuities associated with changes in sensor and/or drift over time.

  ○ For AQUA_MODIS_L3C (2002-2018), significant trends in LST of 0.64-0.66 K/decade are obtained, which compare well with the equivalent T2m trends of 0.52-0.59 K/decade.

❖ The LST_cci v1 MODIS L2 data appear to be several K too cold over the Greenland Ice Sheet when compared to airborne IST observations. There are also occasions where the MODIS data are 30-40 K too cold that do not look like typical cloud contamination, which may represent some error in the processing of these data in this region.

There were known processing bugs in this version of the LST_cci MODIS processor, which have subsequently been addressed by the development team. This may be the cause of the observed 30-40 K cold outliers observed in this UCS. Systematic cloud contamination over ice sheets has also been observed by the Science Team, which have been addressed with the new cloud screening approach in v2.00.

❖ The LST_cci Aqua/Terra MODIS L2 and L3 data appear to be up to a few K too warm over a test site in Spain. This offset is not apparent in the operational NASA MODIS products and may be due to an incorrect surface emissivity being used in the LST_cci products. This relative bias is improved in v2 LST_cci products, but still apparent.

An updated emissivity data set is being implemented in v2.0 of the LST_cci MODIS products. The LST_cci v1.0 products are based on an older emissivity data set and it is expected that the updated version in v2.0 will improve the accuracy of the LST_cci retrievals in this case. Also unlike for the dedicated Validation work stream, the validation at the Spain site was carried out with reduced resolution data and may not ensure best representativeness for the LST_cci data.

❖ The LST_cci multi-sensor L3 (0.05°) products show non-climatic discontinuities due to sensor changes and are therefore not suitable for applications that require data which are homogeneous with time (e.g. trend analysis).
   ○ The ATSR-2 period of the IR multi-sensor CDR appears to be noisier than the AATSR period, particularly for LST_{day}.
   ○ The LSTs from individual sensors that comprise the MW CDR appear to drift with time and there are jumps in the record at sensor transitions.

It should be noted that the time difference correction in the beta version of the IR multi-sensor product was experimental and performed with respect to MODIS as a reference sensor. For this v1.0 product, sensor inter-calibration was not included, which has since shown to have an impact. Furthermore, subsequent analysis has suggested that there may be some drift in the MODIS channels, which is also being addressed. A modified approach will be implemented for the v2.0 product, which is expected to improve the homogeneity of the multi-sensor product significantly. Efforts are also underway to implement a correction for the temporal drift in the MW multi-sensor product, which should be included in the next version of the product.

4.2   Data set improvements, artefacts and issues

Some data set improvements, artefacts and issues have been identified in the beta versions of the LST_cci data sets through several of the UCS, which are summarised below.

❖ For many applications, LSTs without a specific observation time (e.g. because they are produced by averaging over multiple orbits/times) cannot be used. Following feedback on the v1 products, LST_cci L3 IR LSTs produced through averaging over multiple orbits were replaced by LSTs closest to the nominal overpass time of each satellite.
   ○ This has significantly improved the consistency of the LST vs T2m correlation and slope with latitude over Europe and use of the data in machine learning estimates of surface fluxes.
   ○ A recommendation is to provide both instantaneous and averaged LST fields (despite the fact that also the number of ancillary fields on observation time and angles and uncertainties will be multiplied), including hourly data.
❖ There is significant residual cloud contamination in the LST_cci IR products.
   ○ This has been noted in particular for MODIS/Aqua, SEVIRI and ATSR-2 (India only), but all IR products suffer from this issue.

○ If cloud screening cannot be improved, it would be useful to have some guidance for users on this issue on how to remove erroneous data.

Some of the residual cloud contamination in the MODIS data was due to a bug in the LST_cci processor, which has now been resolved. More generally, there is a dedicated project work package on improving cloud screening in LST_cci. A new probabilistic approach to cloud screening has been implemented for the LST_cci MODIS and ATSR V2.0 data releases, which should reduce the cloud contamination further in these products. It is a known issue that ATSR-2 does not have any data over Central Asia and Indian during the mission lifetime due to an in-flight switch-off so there should be no data here. There are no plans to update the cloud mask used in the LST_cci SEVIRI product, but the merged product will include an additional filtering mechanism.

4.3 Data file issues and recommendations

A number of issues relating to the data files themselves have been identified in the beta versions of the LST_cci data sets through several of the UCS, which are summarised below. This list also includes suggestions for other data-file improvements that have been requested by users.

❖ The current method for delivering LST_cci 0.01° is not optimal. Users of these data have had to spend considerable time mosaicking the data together.

○ It would be preferable if the data from each orbit were mosaicked beforehand and provided as tiles, similar to the gridded MOD11/MYD11 data products of NASA

Improved delivery of LST_cci data is currently being developed by the Science Team; a command line tool for re-gridding and sub-setting to user defined resolutions will be available at end of 1st Quarter 2022.

❖ There are discrepancies between the IR and MW product formats. Having a more consistent format between the two product types is preferred. For example:

○ Classification is by day/night for IR but ascending/descending for MW.
○ Provision of quality flags / other information is inconsistent (e.g. no land cover class information is provided in the MW data and no quality flag is provided in the IR data).

Many users prefer day/night classification, which is why this approach has been adopted for the IR data sets. However, it is not possible to classify the MW observations in the same way because the overpass time is ~6-8 am/pm. The differences in quality flags between the two product types arise from the different processing requirements in each case. However, consultation with users will continue on both these points to find the best way forward in each case.

❖ There are some errors in the information provided in the data files:

○ Incorrect information in the global attribute 'platform' in the MULTISENSOR_IRCDR_L3S.
○ 'standard_name' field contents for both latitude and longitude was set to 'latitude' in the v1 products, but this has been corrected in the v2 products.

Both these issues have already been resolved ready for the next product release.

❖ The current land cover class information provided in the LST_cci files is static; provision of dynamic/annual land cover data would be better (note users do appreciate the provision of land cover class data in the LST_cci data files).

Dynamic land cover information will be implemented for future releases of the LST_cci data files.

❖ No emissivity values were provided in version 2 LST_cci MODIS L3C products (unlike in version 1 products); emissivity is a key variable to obtain LST data so should be included.

❖ Provision of satellite view zenith angles with sign (i.e. '-' or '+') that indicates whether the view is towards the east or west (it is noted that this will not be meaningful at very high latitudes but for the majority of the orbit this is useful information). This would be easier for users, who currently have to obtain this information from the satellite azimuth angle, which is an extra step.

❖ The latitude and longitude values of the LST_cci MODIS/ATSR 0.01° products global attributes "geospatial_lat_min", "geospatial_lat_max", "geospatial_lon_min", and "geospatial_lon_max" need to be corrected by half pixel in order to be equal to the actual bounding box coordinates of each LST image. The values currently provided are the latitudes and longitudes of the centre of the four corner pixels. This should be corrected.

❖ Uncertainty information in the LST_cci MSG_SEVIRI_L3U products is only available from mid-2008 onwards, and the first period of available data in the record on uncertainty give negative values.

This is a known processing bug and has been resolved for the next release.

❖ The spatial extent of the SEVIRI disk changes at some point in the record, so only in the later part also north-eastern Europe and parts of south America have valid data. This should be rectified in some way, or at least a guidance note should be issued to users.

❖ The fields 'ncld' and 'variance' in the LST_cci MSG_SEVIRI_L3U products are included in the files but have no meaning as the values are instantaneous and nearest neighbour gridding was performed. As the LST_cci files have a standardised format across all products, it is suggested that a comment is added to inform the user of these non-meaningful fields for SEVIRI in the file attributes.

❖ For the LST_cci 0.01° products, naming the LST_cci data files indicating the geolocation of the data would be helpful, or providing them with a clear identification according to the MODIS tiling system or for example the Sentinel-2 tile grid (UTM system). This would make the identification of tiles containing the LST_cci data over the areas of interest easier.

The new re-gridding and sub-setting to user defined resolutions will better address the requirements from the whole user community.

❖ Provide a 'readme' file in the current public directory for the beta products that includes a list of acronyms and information on the directory structure.

Both a separate ReadME file and a QuickStart in the Product User Guide have been created.

4.4 Other recommendations / future considerations

The following recommendations to consider for future work were suggested in this assessment. It is recognised that some of these are beyond the scope of the current LST_cci project phase, but many will be confronted in Phase-2:

❖ Dedicated effort towards improving IST algorithms should be considered

❖ Extend SEVIRI data record beyond 2008-2010

❖ Implement a geometrical correction to 'adjust' the LSTs to nadir-equivalent LSTs for all sensors

❖

❖ Provide downscaled (higher spatial resolution) SEVIRI data (e.g. downscaled with MODIS)

❖ Provide instantaneous LSTs in L3 products as an extra fields in the LST_cci products (e.g. averaged LSTs over each orbit separately).

❖ Provide infilled LST products where IR data have been used.

❖ Provide LST products for AVHRR/3 and VIIRS.

In addition, it is noted that the uptake of uncertainty information in UCS and other studies is minimal so effort should focus on improving this in the user community. Many of the studies require spatial and/or temporal averaging of the data and therefore require propagation of uncertainty information, which is a non-trivial task. (It takes some weeks or even months to write robust software to re-grid data and propagate uncertainties correctly, which is a major barrier to users). The new re-gridding and sub-setting tool will propagate uncertainties in the LST_cci data sets.

4.5 Feedback from CCI Science Team

The User Case Studies have provided highly relevant feedback for the Science Team to improve the performance of the LST_cci products. The Science Team have in parallel been working on improvements to v2 products, and have taken on-board feedback from the CRG studies throughout the progress of the Use Case Studies. These improvements were made available to the UCS teams, but some UCSs required bespoke data provision not yet available for the v2 products, so have continued assessment of v1 data here.

While the focus of this report is on an independent climate assessment of the LST_cci products it is useful to provide the wider context of how the project is responding to the feedback through close interaction with the CRG. Some of the key advances that have been implemented in V2.00 of the LST_cci products, in response to the majority of the UCS feedback, are summarised below and presented in detail in [AD-01]:

❖ Cloud masking:

○ This has been reported as an issue by the majority of UCS teams and is particularly emphasised for the MODIS product. Evidence suggests this is a result of two different factors:

▪ Use of the operational MODIS cloud mask rather than the new CCI Probabilistic cloud mask which is being implementing across polar-orbiting IR sensors in V2.00

▪ Some processing bugs in V1.00 have come to light following early user feedback, with some months having very bad cloud masking. These bugs have been fixed for in V2.00

○ Cloud screening is also being improved for the CDRs in a dedicated Work Package.

❖ Systematic warm and cold biases in MODIS data:

○ The operational MODIS use the latest emissivity retrievals either direct from multi-channels or indirect from new emissivity data sources. The LST_cci MODIS V1.00 product uses an old emissivity dataset. This difference in input emissivity data is the hypothesised cause of the systematic biases.

- ○ This has been changed in V2.00 such that MODIS now uses the latest CAMEL V2 data which was originally generated from MOD21 and ASTER inputs. The impact of this has been to reduce the systematic bias seen over the validation site in Spain.
- ○ Systematic cloud contamination is seen in offline tests over ice sheets by the Science Team, and is the likely source of the cold bias for these regions. This is being addressed with the new cloud making approach for V2.00

❖ Stability:

- ○ Work by the Science Team have identified [RD-1] temporal drifts in calibration for each MODIS instrument and for each channel of these instruments. Intercalibration corrections have been implemented in V2.00 and should improve the stability of the MODIS products.
- ○ For the ATSR CDR, a time difference correction was implemented in V1.00 which was experimental and performed with respect to MODIS as a reference sensor. No account was made of the inter sensor calibration, which has been shown since to have an impact. It is expected that V2.00 will show an improvement.

❖ Data usage:

- ○ The IR data follows a day / night split for the L3C products. This is consistent with Sea Surface Temperature CCI and this will be maintained for LST_cci.
- ○ Quality flags are only provided in the L3C products for the MW product. This is because these provide additional indication of sub-optimal retrievals. In contrast, the IR data processing for Level-3 has already theoretically filtered out all the problem data, such as cloudy pixels or low confidence pixels, and so the quality level is already expected to be at its highest. However, it is recognised that residual cloud contamination could be identified for the user in a Quality Level indicator; Phase-2 will look at this feasibility.
- ○ Incorrect global attributes reported have been fixed in V2.00
- ○ Several studies have commented on the difficulty in dealing with the customised L3C data. A command line tool for re-gridding and sub-setting to user defined resolutions is being developed to better address the needs of the users.
- ○ In V1.00 land cover was a static auxiliary input dataset. In V2.00 a dynamic approach has been implemented using annual Land Cover CCI as the basis.
- ○ There are however some changes that will not be implemented, since they would be in contradiction with the community established approaches first set out in GlobTemperature and brought forward into LST_cci:
  - ▪ Satellite zenith angles will still be provided as per V1.00. Viewing direction can be acquired already via the satellite azimuth variable.
  - ▪ The geolocation values provided will continue to be the latitudes and longitudes of the centre of the grid-cells.
  - ▪ Suggested downscaling of coarse resolution SEVIRI data is out-of-scope in LST_cci.

End of document